Trends in extreme precipitation and the influence by meteorological parameters following the RCP8.5 scenario over 2 catchments in India

---

Master's Thesis in Climate Dynamics

Ingri Halland Soldal

June, 2015

UNIVERSITY OF BERGEN
GEOPHYSICAL INSTITUTE

Abstract

The Historical1 simulation (1960-2000) and the RCP8.5 scenario (2060-2100) from the NorESM are used to investigate trends in extreme precipitation, as well as the impact from vertical velocity, specific humidity, divergence and temperature on the precipitation formation. The calculations are performed over the Indian catchments Godavari and Krishna, and are restricted to the monsoon season (June-September). Precipitation from the APHRODITE observations are used to validate the NorESM precipitation, and the vertical velocity, specific humidity, divergence and temperature are validated against the NCEP1 reanalysis. The calculated trends in extreme precipitation show that both the yearly mean intensity and the yearly number of events will increase in the future, by approximately 30 % and 40 % (90 % over Krishna), respectively. Using linear regression analysis, the vertical velocity is found to be the most important factor in the formation of extreme precipitation with a correlation of 0.66 over Godavari and 0.47 over Krishna. Along with the specific humidity, most of the precipitation amounts can be accounted for by only including these two parameters, while the temperature is assumed to be less important. A simple model is also applied to estimate precipitation under the assumption that an air parcel follows the moist adiabatic lapse rate. This estimated precipitation is underestimated, and the extreme precipitation has its maximum values 20 mm below the NorESM extreme values. This shows the importance of including diabatic terms such as radiative cooling, which increases the condensation rate of an air parcel.

Acknowledgements

First of all, I would like to thank my supervisor, Asgeir Sorteberg, for guiding me through this thesis. He always made time for my questions and was very helpful in helping me find relevant background information, along with shearing his scripts with me.

I would also like to thank Dr. Ellen Viste for letting me borrow some of her MatLab-scripts and Idar Hessevik for solving my issues regarding disk-space availability.

Another person that really helped me through this work on the personal plan is my husband, Jonas Soldal. Thank you for always being supportive and backing me up during the last five years. I owe you so much!

Last, but no least: all of my fellow students! You made these past 5 years so fun and interesting, and I feel honoured to have met all of you.

Ingri Halland Soldal,

02/06/2015

Content

1. Introduction

The Indian monsoon is a yearly phenomenon that affects more than one billion people (Turner and Annamalai, 2012). It contains large amounts of precipitation, and is responsible for 74.2 % of the annual rainfall in India (Attri and Tyagi, 2010). Over the years, the monsoon has been very reliable, and the farmers have used their experience to schedule the times of sowing and harvesting. With earlier monsoon onset dates and delays in monsoon offset dates in the future (Kitoh et al., 2013), the farmers will have less control over the precipitation cycle, and either the crops will dry out due to a lack of expected water, or they will be destroyed by sudden intense precipitation. Both outcomes cause an enormous challenge to the food availability and will affect the Indian economy.

The Indian monsoon occurs during the northern hemisphere summer months (June-September) and develops from pressure differences between the Asian continent and its surrounding oceans. Because the heat capacities are different between soil and water, the increased solar insolation during late Spring and Summer heats up the continent more than the ocean, developing a pressure gradient from ocean to land. This pressure gradient causes an atmospheric circulation where moist air is transported cross-equatorial from the Indian Ocean into the Asian continent (Figure 1.1., a). Due to the presence of orography by i.e. the Western Ghats and the Himalayas, and to the heating over the continent, the incoming air is forced to ascend, in which it cools before condensation and finally precipitation occurs. As the air condensates it releases latent heat, which warms the air and increases the pressure aloft. This latent heat release is absent over the ocean, in which the upper-level pressure will be lower than over the continent. This creates a pressure gradient from the continent to the ocean aloft, which develops into a return flow (Figure 1.1, b).

The above description of the Indian monsoon is the basic theory that has been proposed all the way back to Halley in 1686. A more complicated version includes the effect by the Tibetan Plateau, which is highly debated. Ueda and Yasunari (1998) suggests that the plateau contributes with diabatic heating to the upper levels of the troposphere, which enhances the meridional temperature gradient and makes it possible to extend through most of the column. This result would lead to a stronger monsoonal flow. However, an experiment performed by Boos and Kuang (2010), where in one case the topography of the plateau was completely removed, and in another the plateau was replaced with a narrow mountain range, showed that the Tibetan Plateau is important for the nearby areas as the precipitation and upper-level

temperatures weakened without its presence, while it has minor influence on the large scale Indian monsoon circulation. Due to the complexity of the monsoon, there is also a suggestion that the monsoon is caused by the seasonal northward shift of the intertropical convergence zone (ITCZ), as the temperature gradient cannot explain all the aspects of the monsoon by itself (Privé and Plumb, 2007).

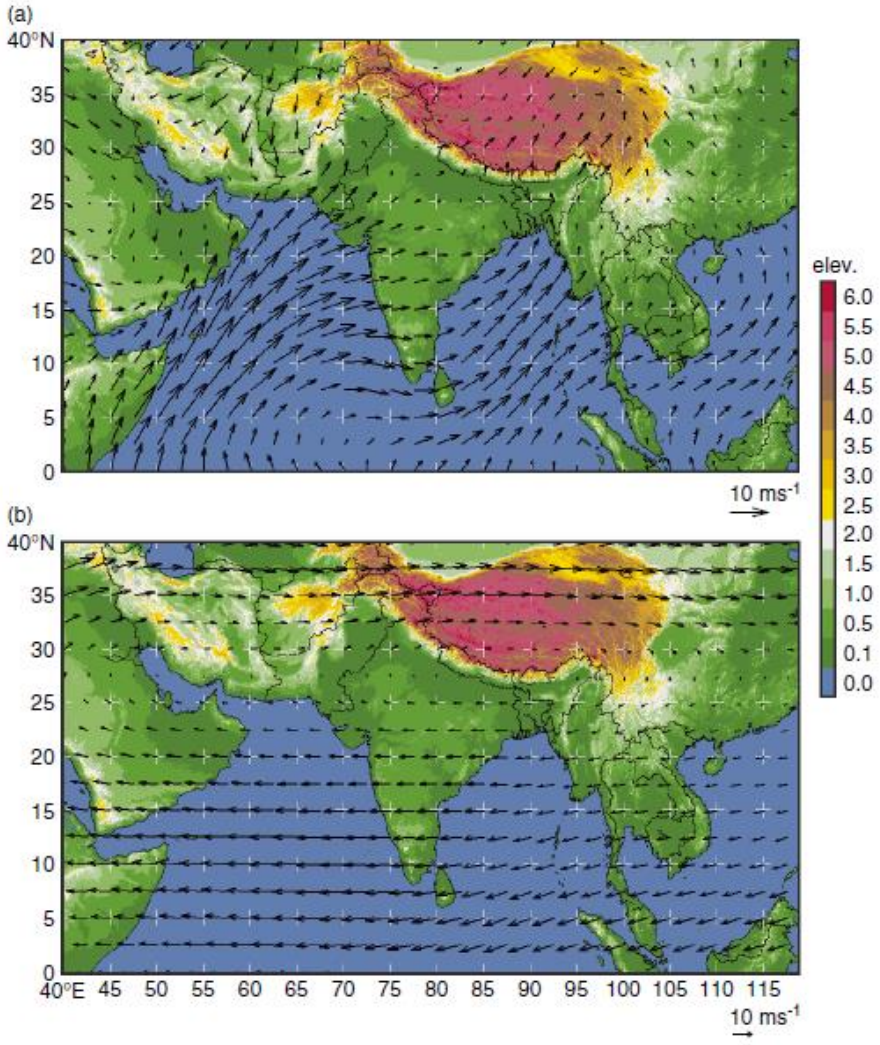

Figure 1.1: The mean winds during the Summer monsoon for a) 1000 hPa, and b) 200 hPa superimposed on topography. The elevation has units of km. The figure is retrieved from Houze et al. (2007).

Today's research has much of its focus shifted towards how the monsoon will change in the future. Ueda et al. (2006) investigated how an increase in greenhouse gases will affect the Asian Summer Monsoon. Due to a resulting increase in atmospheric temperatures, the water vapour content will enhance as well (as warmer air can hold more water vapour), and the precipitation amounts will increase. However, due to the absorption of solar insolation by the

greenhouse gases, the temperature in the middle troposphere will also enhance, stabilizing the vertical profile and weaken the circulation.

Concerning the water vapour content via the Clausius-Clapeyron relation, O'Gorman and Muller (2010) found that the (saturation) column water vapour will increase with ~8 % K^{-1} at 30 °N. Pall et al. (2007) further coupled this to the future change in extreme precipitation, concluding that the extreme precipitation was closer to the Clausius-Clapeyron constraint than to the change in mean precipitation (change in mean precipitation data tends to equal zero or have opposite sign compared to higher percentile data). Pall also suggests that the deviations in the calculations of extreme precipitation change compared to Clausius-Clapeyron scaling comes from dynamic factors such as a change in the circulation.

In this thesis, the change in 6-hourly extreme precipitation intensity during monsoonal months between the climatological means of the periods 1960-2000 and 2060-2100 is studied. An event is classified as extreme if its value exceeds the 99.5 percentile of all data in its grid point. Two catchments within India are investigated; Godavari and Krishna (see fig.1.2), which are the catchments areas of two of the biggest rivers in India. By using multiple linear regression, the dependence of extreme precipitation on meteorological parameters is investigated, and the change in the vertical profile of both dynamic and thermal variables with increased greenhouse gases is compared to the change in extreme precipitation. Finally, the complexity in the creation of extreme precipitation is investigated by using a simple model only including moist adiabatic ascent. These analyses and comparisons will provide sufficient information to answer the main research questions:

- Which meteorological parameters are most important in the formation of extreme precipitation during the monsoon?
- Which meteorological parameters will be most important in the formation of extreme precipitation during the monsoon in a climate affected by increased greenhouse gases?
- How complex is the process of creating extreme precipitation, i.e. is the process as simple as only involving moist adiabatic ascent?

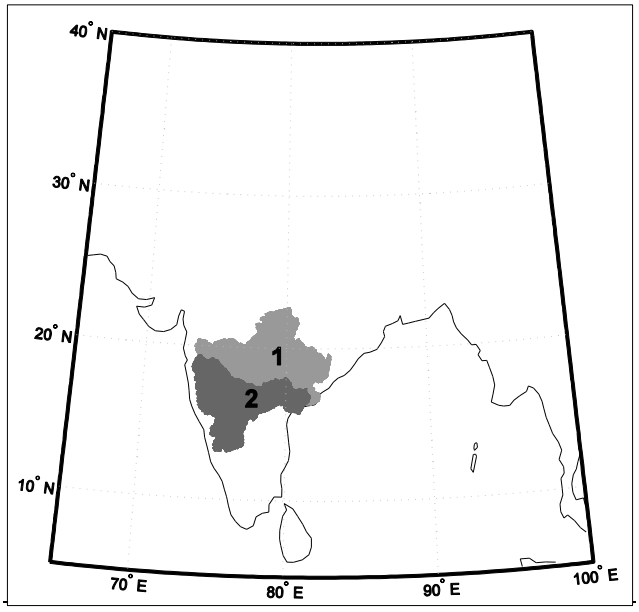

Figure 1.2: The two regions studied in India: 1) Godavari and 2) Krishna.

Chapter 2 goes through the theory of the Clausius-Clapeyron relation, the calculation of vertical velocity, the column integrated water vapour, and convective available potential energy. Chapter 3 gives the relevant statistics used in the thesis. A description of the applied data is shown in Chapter 4, followed by the validation data in Chapter 5. In Chapter 6, the results regarding the means and changes in extreme precipitation, and in the meteorological parameters, are presented, before the simplified precipitation model is presented in Chapter 7. Chapter 8 contains discussion including a multiple regression analysis, and finally Chapter 9 and 10 gives a summary with concluding remarks and possible further work, respectively.

2. Theory

2.1 CLAUSIUS CLAPEYRON RELATION

The Clausius-Clapeyron equation is given by

$$\frac{de_s}{dT} = \frac{L_v}{T\Delta V} \tag{2.1}$$

where L_v is the latent heat of evaporation, e_s is the saturation vapor pressure, T is the temperature and V is the molecular volume. If we integrate Equation 2.1, and introduce the ideal gas law

$$e_s \cdot V = R_v \cdot T \tag{2.2}$$

where R_v is the gas constant for water vapor, we get

$$ln\left(\frac{e_{s1}}{e_{s2}}\right) = \frac{L_v}{R_v}\left(\frac{1}{T_1} - \frac{1}{T_2}\right) \tag{2.3}$$

Given that T_1=273 K and $e_{s2}(273K) = 6.11hPa$, the equation becomes

$$e_s(T) = 6.11hPa \cdot \exp\left(\frac{L_v}{R_v} \cdot \left(\frac{1}{273K} - \frac{1}{T}\right)\right) \tag{2.4}$$

which gives an exponential relationship between water vapour and temperature (Wallace and Hobbs, 2006).

In the atmosphere, the range of temperatures studied are relatively small, and to a good approximation Equation 2.1 together with Equation 2.2 can be applied as

$$\frac{\Delta e_s}{e_s} = \frac{L_v}{R_v T^2} \cdot \Delta T \tag{2.5}$$

(Wallace and Hobbs, 2006), giving an approximately linear relationship between the fractional rate of change of water vapour and the suggested temperature change (see Figure 2.1). For a 1 K increase at T=300 K, using $L_v = 2.5 \cdot 10^6$ J kg^{-1} and $R_v = 461$ J K^{-1} kg^{-1}, the relative change in water vapour, obtained by multiplying Equation 2.5 by 100%, show an increase of ~6%.

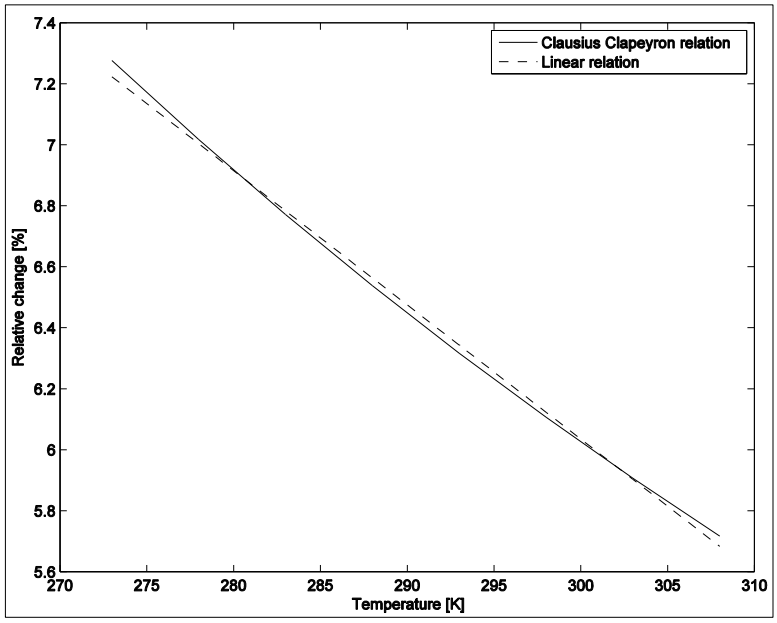

Figure 2.1: For a small temperature range, the relative change in water vapour content due to a 1 K increase in temperature is approximately linear through the Clausius-Clapeyron relation.

2.2 VERTICAL VELOCITY

The vertical velocity can be calculated through three different methods; the kinematic method, the adiabatic method, and through the omega equation. In this thesis, the vertical velocity is calculated using the kinematic method, which means that it is only dependent on divergence of the horizontal winds.

The continuity equation is given by

$$\frac{\partial \rho}{\partial t} = -\nabla(\rho \vec{v}) \tag{2.6}$$

where ρ is the density of the air, t is time, $\vec{v} = (u, v, w)$ is the velocity vector, and $\nabla = \left(\frac{\partial}{\partial x}, \frac{\partial}{\partial y}, \frac{\partial}{\partial z}\right)$. Assuming that ρ is constant, the equation transforms into

$$\frac{\partial u}{\partial x} + \frac{\partial v}{\partial y} + \frac{\partial w}{\partial z} = 0 \tag{2.7}$$

Using the hydrostatic equation

$$\frac{\partial p}{\partial z} = -\rho g \tag{2.8}$$

and that

$$\omega = \frac{dp}{dt} = \frac{dp}{dz}\frac{dz}{dt} = \frac{dp}{dz} \cdot w \tag{2.9}$$

Equation 2.7 transforms into

$$\frac{du}{dx} + \frac{dv}{dy} + \frac{d\omega}{dp} = 0 \tag{2.10}$$

where u is the horizontal velocity in the x (zonal) direction, v is the horizontal velocity in the y (meridional) direction, ω is the vertical velocity in pressure coordinates and p is the pressure level. Rearranging the equation, it becomes

$$\frac{d\omega}{dp} = -\left(\frac{du}{dx} + \frac{dv}{dy}\right) \tag{2.11}$$

which can be approximated as:

$$\omega_k = \omega_{k-1} + \left(\frac{du}{dx} + \frac{dv}{dy}\right) \cdot (p_{k-1} - p_k) \tag{2.12}$$

where k=1 : K, and K is the final level of the pressures. The vertical velocity at the surface, ω_0, is sat equal to zero.

The second term in Equation 2.12 is called the divergence term. Since the pressure difference is taken between k and k-1, this term is located in the middle of each two layers, while ω is located at each layer. It will therefore be an uncertainty in this term, which will accumulate upwards in the atmosphere, and the calculated ω_k might be too high or too low due to this numerical uncertainty. To solve this issue, the O'Brien adjustment factor (O'Brien, 1970) is applied. The O'Brien adjustments factor is based on selecting a pressure level high up where the vertical velocity is set to a prescribed value (usually zero). It is also assumed that the uncertainty/error is distributed uniformly over all the divergence estimates, i.e. for all levels. The corrected ω will then be:

$$\omega'_k = \omega_k - \frac{k \cdot (k+1)}{K \cdot (K+1)} \cdot (\omega_K - \omega_T) \tag{2.13}$$

where ω_T=0 is the vertical velocity at the selected top pressure level. This will give a very low correction near the ground, but it will increase upward in the atmosphere (O'Brien, 1970).

To include topography in the vertical velocity we have to add a terrain-induced omega-term. This is done following Sinclair (1994):

$$\omega_{Total,k}(p) = \omega'_k + \omega_s \cdot \left(\frac{p_k - p_t}{p_s - p_t}\right)^{tan(\gamma \cdot \frac{\pi}{4})} \quad (2.14)$$

where p_k is the pressure at level k, $p_t = 100\ hPa$ is the selected pressure level at the top of the column, p_s is the surface pressure level and γ is a parameter between 0 and 2 to decide how fast ω_s will reach zero upward in the atmosphere. γ is chosen to obtain the best results when estimating precipitation amount in the full model, but in general we have that $\gamma = 1$ gives a linear decrease, $\gamma < 1$ gives a slow decrease, while $\gamma > 1$ gives a rapid decrease. For γ=2 we get the same results as with no topography. ω_s is the topography-generated near-surface omega, and is calculated based on the slope of the topography and the near surface winds (u_s and v_s, taken as the mean horizontal winds in the bottom two layers):

$$\omega_s = -\rho_s g \cdot \vec{V_s} \cdot \nabla z_s = -\frac{p_s g}{R_d T} \cdot \left(\frac{du_s}{dx} + \frac{dv_s}{dy}\right) \quad (2.15)$$

where g is the gravitational acceleration, T is near surface temperature, ρ_s is the surface air density, and R_d is the gas constant of dry air (Sinclair, 1994).

2.3 INTEGRATED WATER-VAPOR TRANSPORT AND HORIZONTAL DIVERGENCE

The integrated water vapour transport is calculated using the horizontal velocity, $\overrightarrow{v_h}$=(u,v), and the specific humidity, q:

$$Tr = \sqrt{\left(\int_{p_s}^{p_t} u \times q \ dp\right)^2 + \left(\int_{p_s}^{p_t} v \times q \ dp\right)^2} \quad (2.16)$$

p_s and p_t are the pressures at the surface and at the top of the integrated column, respectively. To calculate these integrals the trapeze method is used

$$\int_1^n f(x)\,dx \approx (n-1)\left[\frac{f(1) + f(n)}{2}\right] \quad (2.17)$$

To improve the result, the integral is divided into equally spaced levels in between level 1 and n, before adding them together to receive the final value:

$$\int_1^n f(x)\,dx \approx \frac{n-1}{2}[f(1) + 2f(i+1) + \cdots + 2f(n-1) + f(n)] \quad (2.18)$$

(Adams and Essex, 2009).

From Equation 2.10 the horizontal divergence is given by

$$\nabla \cdot \overrightarrow{v_h} = -\frac{d\omega}{dp} = \frac{du}{dx} + \frac{dv}{dy}. \quad (2.19)$$

Positive divergence is referred to as an increase in volume and is associated with downdrafts. Negative divergence, or convergence, is referred to as a decrease in volume and is associated with updrafts (Harwood, 2006).

2.4 CONVECTIVE AVAILABLE POTENTIAL ENERGY

Convective available potential energy (CAPE) is the available energy stored between the level of free convection (LFC) and the equilibrium level (EL) in the atmosphere. The LFC is the height where the parcel gets warmer than the environment, and the EL is the height where the temperature of the parcel equals that of the environment above the LFC (Markowski and Richardson, 2011). The CAPE increases as the difference between an air parcel and the surrounding air increases, and is proportional to the kinetic energy that can be added to the vertical velocity by buoyancy. If the CAPE grows large enough (typically > 2500 J/kg) and is released, single-cell convection can occur, creating large amounts of precipitation for a short time (Markowski and Richardson, 2011).

To calculate CAPE it is important to use the virtual temperature (virtual potential temperature) instead of temperature (potential temperature) because the moisture increases the CAPE by about 10 percent, as well as reducing the Convective Inhibition (CIN) (Markowski and Richardson, 2011). This may lead to a total different result from the same calculation excluding moisture effects. CIN is defined as negative CAPE, and equals the energy required to lift a parcel of air to its LFC. The CIN is necessary for the build-ups of energy for deep convection to occur, but if the CIN becomes too large (i.e. >100 J kg^{-1}) the air parcel may not be able to reach its LFC and the deep convection will be absent (Wallace and Hobbs, 2006).

The equation used to calculate CAPE is given by

$$CAPE = \int_{z=z(LFC)}^{z=z(EL)} \frac{g}{\theta} \Delta\theta_v(z) dz \quad (2.20)$$

where z(EL) and z(LFC) are the heights of the equilibrium level and the level of free convection, respectively, g is the gravitational constant, θ is the potential temperature and

$\Delta\theta_v(z)$ is the change in virtual potential temperature between the two levels (Stull, 1988). By using the hydrostatic equation (Equation 2.8) (Wallace and Hobbs, 2006), the CAPE formula in pressure coordinates will be

$$CAPE = \int_{p(EL)}^{p(LFC)} \frac{1}{\rho\theta} \Delta\theta_v(p)dp \tag{2.21}$$

θ and θ_v is found using the equations

$$\theta = T \cdot \left(\frac{p_0}{p}\right)^{0.286} \tag{2.22}$$

and

$$\theta_v = \theta \cdot (1 + 0.61 \cdot w) \tag{2.23}$$

where p_0 is the reference pressure and w is the mixing ratio (Stull, 1988), which in this case is assumed equal to the specific humidity, q (Wallace and Hobbs, 2006). The density, ρ, is calculated at each pressure level using the ideal gas law per unit mass:

$$\rho = \frac{p}{R_v T} \tag{2.24}$$

with p being the pressure level, T the temperature at that level, and R_v the gas constant for water vapour.

3. Statistics

Several statistical procedures have been applied within this master thesis. To calculate the historical trends both linear regression and the Sen's slope test were performed, and linear regression was used to study the variability in extreme precipitation. The Mann-Kendall trend test, the bootstrapping method and the F-test were used to calculate the significance of the aforementioned trends.

3.1. LINEAR REGRESSION

In linear regression, you calculate the relationship between a dependent variable and one or several independent variables. The regression equation is given by

$$Y = \frac{\partial Y}{\partial X_1} \cdot X_1 + \frac{\partial Y}{\partial X_2} \cdot X_2 + \cdots + \frac{\partial Y}{\partial X_n} \cdot X_n + b_0 \tag{3.1}$$

where $X_1, \dots, X_n$ indicate each of the independent variables and b_0 is the y-intercept value. If n=1, Equation 3.1 turns into a linear equation on the form

$$Y = \frac{\partial Y}{\partial X} \cdot X + b_0 \tag{3.2}$$

The multiple linear regression is performed both directly from Equation 3.1 and as a standardized equation using the formula

$$X_{STD,n} = \frac{X_i - \mu}{SD(X)} \tag{3.3}$$

for each n. Here X_i is each element in variable X, μ is the mean of variable X and SD(X) is the standard deviation of X. This standardization is also performed on the dependent variable, Y. When using standardized variables in the regression they are all expressed in units of standard deviations, and it is thus easier to say something about which is the most important factor in inducing variability in the dependent variable. The results we get from Equation 3.1 only gives us the value for that specific factor and its unit, and it is thus hard to compare it to the other factors. The one limitation when using the regression values is that the factors have to be independent, i.e. they cannot be correlated with one another.

3.2. SEN'S SLOPE

The Sen's slope is an alternative way of calculating the trend in the data. In this statistic, you calculate the slope b by taking the median (50th percentile) of all slopes given by

$$\frac{y_j - y_i}{x_j - x_i}, \qquad \begin{cases} j = 1:n \\ i = 1:n \end{cases} \quad j \neq i \tag{3.4}$$

where all sample pairs have been used. When b is calculated, one can calculate the y-intercept by taking the median of $y_i - bx_i$ (Sen, 1968). By taking the median of all the calculated slopes within the dataset, the benefit of the model is that it is quite robust against the outliers (Hirsch et al., 1982).

3.3. SIGNIFICANCE TESTING

When a dataset is statistical significant it means that the calculated p-value is less than the chosen significance level, where the significance level is the probability of rejecting a null-hypothesis that is true. As an example, if your null hypothesis states that the change in a variable is greater than zero, it will be significant if both ends of your confidence interval (which are selected by the significance level) are greater than zero.

The significance tests in this thesis have been performed using the non-parametric Mann-Kendall- and Bootstrapping trend tests and the parametric F-test. The reason for choosing non-parametric tests for parts of the significance testing is that the data are not necessarily normally distributed, and in addition the selected methods are more robust against outliers. A study performed by Yue and Pilon (2004) also concluded that non-parametric tests for non-normal distributed data have a higher power than parametric tests do, which means that the non-parametric tests have higher probability of correctly rejecting the null hypothesis when it is false. However, when using the linear regression analysis to calculate extreme precipitation variability in Section 8.1, the estimated values are very close to being normally distributed and the F-test is therefore applied.

3.3.1. Mann-Kendall Trend Test

The Mann-Kendall trend test is a test of the significance of the trend found via the calculation of the Sen's slope. For each (x_i,y_i) throughout the dataset, you compare it to the next pair (x_{i+1},y_{i+1}). For each of these comparisons you get a value S equal to 1, 0, or -1:

$$S = \begin{cases} 1, & (x_i, y_i) > (x_{i+1}, y_{i+1}) \\ 0, & (x_i, y_i) = (x_{i+1}, y_{i+1}) \\ -1, & (x_i, y_i) < (x_{i+1}, y_{i+1}) \end{cases} \quad (3.5)$$

Finally, you add up all these S's and use them in the calculation of the standard test statistic Z_s:

$$Z_s = \begin{cases} \frac{S-1}{\sigma} & for\ S > 1 \\ 0 & for\ S = 0\ , \\ \frac{S+1}{\sigma} & for\ S < 1 \end{cases} \quad (3.6)$$

where

$$\sigma^2 = \frac{n(n-1)(2n+5) - \sum t_i(t_i-1)(2t_i+5)}{18} \quad (3.7)$$

n is the total number of data points, and t_i is the number of ties ($x_i=x_{i+1}$ or $y_i=y_{i+1}$) to the extent of i. If $|Z_s| > Z_{\alpha/2}$, where α is the significance level, then the trends is implied to be significant. A strength of this test is that outliers do not affect Z_s as it does not depend on the data values, only their relationships with another.

3.3.2. Bootstrapping

Bootstrapping is a useful technique in cases where it is difficult or even impossible to measure all individuals in a population, i.e. mean size of fish in an area, average age of all people in the world, etc. To solve this issue, bootstrapping uses a resample technique, which means that a sample J of size N is selected from the population, and from J a new sample I of the same size N is created through sampling with replacement. For example, if the lengths of several fish are (in cm) [15 22 18 27 25 30 45], than one resample might be [22 25 30 18 25 45 22]. This resampling is performed a high number of times, i.e. between 1000 and 10 000 times, and for each sample the relationship you are interested in is calculated (the mean, difference between two populations, etc.). Finally, all the values calculated are represented in a histogram, presenting the most likely value (the value calculated most times through all resamples).

To calculate the confidence interval (CI) of these data, the percentile method has been used. This method use the percentile of the data as the upper and lower limits of the CI, i.e. n*(1-α/2) and n*(α/2), respectively, where n is the number of resamplings and α is the significance level.

3.3.3. F-test for Regression

Assuming the regression data has an F-distribution, the F-test can be used to calculate the significance between two variables. The null-hypothesis, H_0, is given by

H_0: $\frac{\partial Y}{\partial X_1} = \frac{\partial Y}{\partial X_2} = \ldots = \frac{\partial Y}{\partial X_{p-1}} = 0$,

i.e. all the slopes in Equation 3.1 vanish, and the dependent variable Y only depends on the intercept value. The alternative hypothesis, H_1, is that the dependent variable Y depends on at least one of the dependent variables:

H_1: $\frac{\partial Y}{\partial X_j} \neq 0$, for at least one value of j.

Assuming that the null-hypothesis is true, the F-test is calculated by

$$F = \frac{\sum_{i=1}^{n}(\hat{y_i} - \bar{y})^2/(p-1)}{\sum_{i=1}^{n}(y_i - \widehat{y_i})^2/(n-p)} \tag{3.8}$$

Here n is the number of observations, p is the number of regression parameters (including the intercept value b_0), y is the observed dependent value and $\hat{y}$ the calculated (regressed) value. The sum in the numerator is called the explained sum of squares (ESS), while the sum in the denominator is called the sum of squares for errors (SSE). (p-1) and (n-p) is the degrees of freedom of the ESS and the SSE, respectively.

The value obtained for F in Equation 3.8 can be located in an F-table along with its two degrees of freedom, and thus the confidence interval and the p-value can be calculated. If the value F lays outside the confidence interval (or the p-value > 0.05, assuming a significance level of 5 %) the null-hypothesis is rejected which implies some degree of dependency between the dependent and independent variable(s).

3.4. VALIDATON STATISTICS

3.4.1. Precipitation

For each month, j, the mean over all values per grid point is calculated:

$$\overline{Pr}(i,j) = \frac{1}{T}\sum_{t=1}^{T} Pr_j(i,t) \tag{3.9}$$

where T is the number of values in one month. From Equation 3.9, the mean over all grid points per month is calculated, leaving us with one value per month:

$$\overline{Pr}(j) = \frac{1}{I}\sum_{i=1}^{I} \overline{Pr}(i,j) \tag{3.10}$$

where I is the number of grid points.

Finally, the result from Equation 3.10 is used to calculate the relative difference between the observed and the modelled data:

$$Pr_{rel.diff} = \frac{\overline{Pr}_{mod}(j) - \overline{Pr}_{obs}(j)}{\overline{Pr}_{obs}(j)} \cdot 100\% \tag{3.11}$$

3.4.2. Temperature and Horizontal Divergence

For the validation of horizontal divergence and temperature, the vertical component of the data has to be included in the calculations. Here it is shown for divergence, but the same equations applies for temperature.

For each month, j, the mean over all values per grid point, i, per pressure level, k, is calculated:

$$\overline{Div}(i,k,j) = \frac{1}{T}\sum_{t=1}^{T} Div_j(i,k,t) \tag{3.12}$$

where T is the number of values in one month. From Equation 3.12, the mean over all grid points per pressure level per month is calculated:

$$\overline{Div}(k,j) = \frac{1}{I}\sum_{i=1}^{I} \overline{Div}(i,k,j) \tag{3.13}$$

where I is the number of grid points.

Finally, the result from Equation 3.13 is used to calculate the difference between the observed and the modelled data:

$$Div_{diff} = \overline{Div}_{mod}(k,j) - \overline{Div}_{obs}(k,j) \tag{3.14}$$

and the relative difference:

$$Div_{rel.diff} = \frac{\overline{Div}_{mod}(k,j) - \overline{Div}_{obs}(k,j)}{|\overline{Div}_{obs}(k,j)|} \cdot 100\% \tag{3.15}$$

3.4.3. Mean absolute percentage error

The mean absolute percentage error is used as an estimate for the accuracy between observed and forecasted/modelled values. If A is the actual value, P is the predicted value, n is the total number of time steps, t, and k represent the pressure level, then

$$MAPE(k) = \frac{1}{n}\sum_{t=1}^{n}\left|\frac{A(t,k) - P(t,k)}{A(t,k)}\right| \cdot 100\% \tag{3.16}$$

4. The data

4.1. NORESM

The following text is retrieved from Bentsen et al. (2013) unless otherwise stated.

In this thesis, atmospheric data from climate simulations contributed by the core version of the Norwegian Earth System Model (NorESM1-M) to the Coupled Model Intercomparison Project Phase 5 (CMIP5) has been used to investigate historic and future parameters over India. These data has a horizontal resolution equal to 2 degrees and the vertical structure is divided into 26 levels with the top level being at 2.917 hPa.

The NorESM is based on the Community Climate System Model version 4 (CCSM4), but differs in that NorESM uses an isopycnic coordinated ocean general circulation model; the atmospheric part is modified by the chemical-aerosol-cloud-radiation interface developed for the Oslo version of the Community Atmosphere Model (CAM4-Oslo); and the biogeochemical ocean module comes from the HAMburg Ocean Carbon Cycle (HAMOCC) model.

To use NorESM to model future changes in climate, it is important to use observed values of solar radiation, volcanic activity, and atmospheric concentrations of i.e. greenhouse gases and aerosols in the simulations to gain the most accurate and reliable results. The model has thus been `spun up` for 700 years with the atmosphere, ice and land component having their initial conditions from the CCSM4 model, and the ocean component was initialized with zero velocities and temperature and salinity values from the Polar Science Centre Hydrographic Climatology (PHC) 3.0. At year 700, the spin-up results was set as initial conditions for the simulations starting in the year 1850, and three historical simulations were run. The run for the period 1850-2012 is used in this thesis (named Historical1).

From the year 2005, four different Representative Concentration Pathways (RCPs) were run: RCP2.6, RCP4.5, RCP6.0 and RCP8.5. These are different scenarios where the radiative forcing, emission rates and emission concentrations are key parameters, and each of the numbers in their names stands for their approximate radiative forcing by the year 2100 (in Wm^{-2}). RCP2.6, -4.5, and -6.0 are all scenarios where the emission concentrations stabilizes when approaching 2100, while RCP8.5 continues with a linear increase (Wayne, 2013). In NorESM, all RCPs, except RCP4.5, runs until 2100, whilst RCP4.5 continues until 2300. The

structure of the model run can be seen in Figure 4.1. For the investigation of future data, the RCP8.5 scenario is used in this thesis.

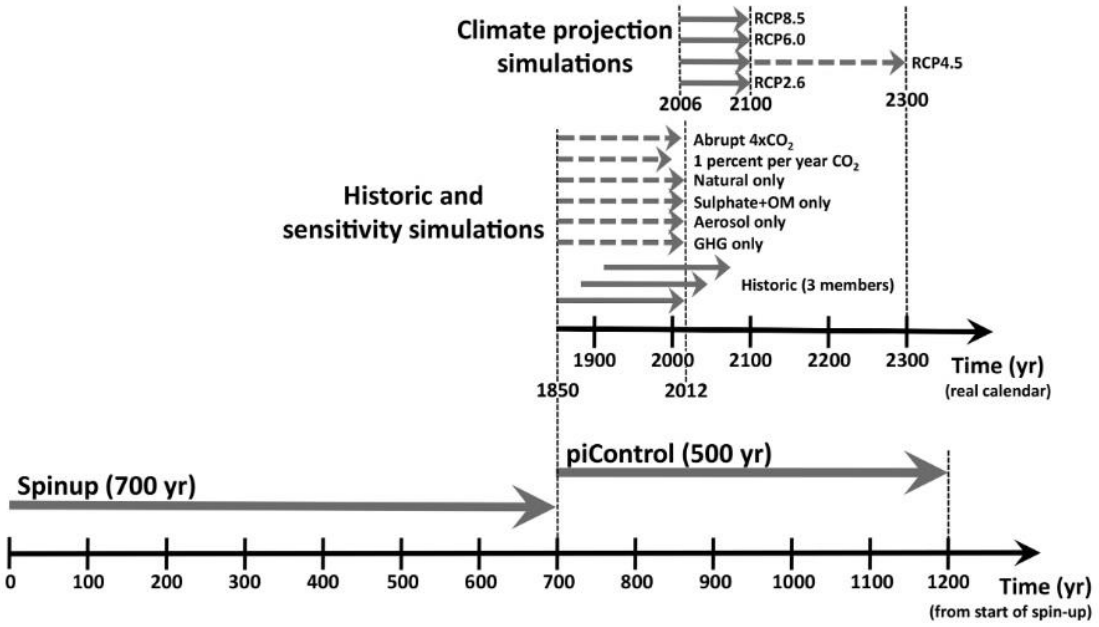

Figure 4.1: A schematic representation of the different simulations and scenarios in the NorESM. At the bottom is the spin-up timeline, and further up, from 1850 and onwards is the calendar timeline (Fig.1, Bentsen et al., 2013).

4.2. APHRODITE

APHRODITE (Asian Precipitation Highly-Resolved Observational Data Integration Towards Evaluation) is a gauge based data set containing daily and climatological (monthly) precipitation data over Asia for the period 1951-2007. The data in APHRODITE is collected from APHRODITE's own database; from data collected by other projects; and from daily global data (Yatagai et al., 2012). The data has a grid point resolution of 0.25°-0.5° (Yasutomi et al., 2011), and due to the use of rain gauges, the data only cover land areas.

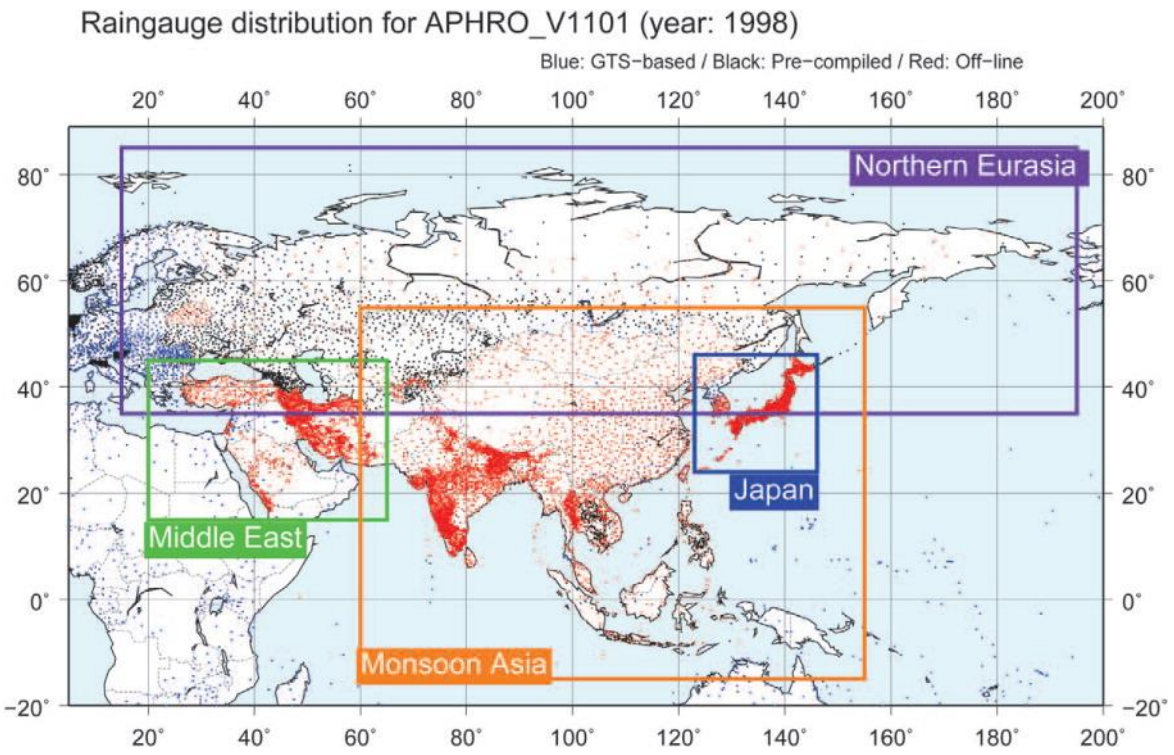

Figure 4.2: Rain gauge distribution over the areas Monsoon Asia, Middle East and Northern Eurasia in the year 1998. Red dots are stations from APHRODITE's individual data collection, blue dots are from the GTS network, and black dots are from precompiled datasets (Fig.1, Yatagai et al., 2012). As can be observed, approximately all data over India are from the individual data collections of APHRODITE.

4.3. NCEP1 REANALYSIS

In a reanalysis, observational data are assimilated and adapted to a numerical weather prediction model (Uppala et al., 2005). The National Centers for Environmental Prediction (NCEP) Reanalysis 1 project consist of instantaneous data of air temperature, geopotential height, relative and specific humidity, omega, and horizontal velocities (u and v). The motivation for the project was to investigate the climate change and thus improve the forecasts (Kalnay et al., 1996).

The reanalysis contains 6-hourly, daily and monthly observations from 1948 to present, in addition to monthly means over the period 1981-2010. It covers the entire globe and has a horizontal resolution of 2.5° × 2.5°, and contains 17 pressure levels (1000, 925, 850, 700, 600, 500, 400, 300, 250, 200, 150, 100, 70, 50, 30, 20 and 10 hPa). For the vertical velocity, the vertical extent stops at 100 hPa (ESRL, 2015).

The observational data in the NCEP1 project is collected from organizations all over the world, and is collected from rawinsondes, ships, buoys, ocean stations, aircrafts, constant-pressure balloons, surface land synoptic data, and from satellites (Kalnay et al., 1996). In this thesis, the vertical velocity, winds, specific humidity and temperature have been used for validation with NorESM data.

5. Validation

Initially, five catchments of India were included in this thesis; Godavari, Krishna, Brahmaputra, Indus and Ganges. Due to poor data-simulations compared with observations and reanalysis data, only Godavari and Krishna will be analysed further.

5.1. PRECIPITATION

The NorESM1-M (hereafter only called NorESM) Historical1 simulated precipitation data is validated against the observationally based APHRODITE data. The validation is based on daily precipitation data from June to September over the years 1960-2000, and includes both an investigation of mean data and of the extreme events (defined as the events above the 99.5 percentile precipitation), as well as the trends in extreme precipitation over the historic period 1960-2000. The reason for not validating for 6-hourly data as this is used throughout the thesis, is due to the lack of observations at this time scale. To calculate the differences between the modelled and the observed data, equations 3.9 through 3.11 is used.

In general, most of the precipitation over India during the monsoon falls along the west coast and along the southern side of the Himalayas (Figure 5.1). Comparing APHRODITE to NorESM, the locations with highest amounts of precipitation are underestimated in NorESM, while for the places with smaller amounts of precipitation NorESM overestimates the precipitation. On the other hand, the resolution in NorESM is much coarser than in the APHRODITE dataset, resulting in a less detailed precipitation pattern for NorESM and possible exclusion of local effects in the simulations.

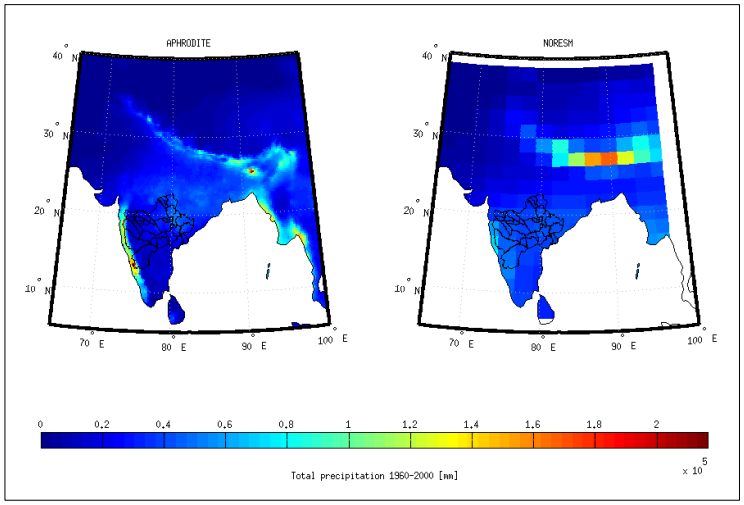

Figure 5.1: Total amount of precipitation (mm) through the months June to September over the period 1960-2000 for left) APHRODITE, and right) NorESM data.

5.1.1 Mean data

The validation over Godavari and Krishna is presented in Table 5.1 and 5.2, respectively. In Godavari, the mean precipitation is overestimated over all monsoon months except June, which is underestimated by 32 %. The largest deviation is found in September with 50 % more precipitation than in APHRODITE. For the 99.5 percentile precipitation, NorESM is underestimated in all months, with September having the largest deviation of -44.3 %. The validation for Krishna shows that the model overestimates the precipitation over the whole period for both the mean and the 99.5 percentile precipitation. The mean precipitation is nearly doubled in July and August compared to APHRODITE, while in July the values are overestimated close to 2.5 times. For the 99.5 percentile the deviations are smaller, with a range between 3 % (August) and 18 % (June).

Table 5.1: Daily validation data in Godavari during the monsoon months (June-September) over the period 1960-2000. The APHRODITE observations are used for comparison with the NorESM Historical1 simulation.

Month:	Mean pr. APHRODITE [mm day^{-1}]:	Mean pr. NorESM [mm day^{-1}]:	Rel. difference mean pr. [%]:	Mean 99.5 percentile pr. APHRODITE [mm day^{-1}]:	Mean 99.5 percentile pr. NorESM [mm day^{-1}]:	Rel. difference 99.5 percentile pr. [%]:
Jun	4.8	3.2	-32.2	76.7	60.5	-21.2
Jul	8.3	9.1	9.7	81.3	56.2	-30.8
Aug	8.2	11.1	35.4	80	65.7	-17.9
Sep	5.2	7.8	50	70.8	39.5	-44.3

Table 5.2: Daily validation data in Krishna during the monsoon months (June-September) over the period 1960-2000. The APHRODITE observations are used for comparison with the NorESM Historical1 simulation.

Month:	Mean pr. APHRODITE [mm day^{-1}]:	Mean pr. NorESM [mm day^{-1}]:	Rel. difference mean pr. [%]:	Mean 99.5 percentile pr. APHRODITE [mm day^{-1}]:	Mean 99.5 percentile pr. NorESM [mm day^{-1}]:	Rel. difference 99.5 percentile pr. [%]:
Jun	3.5	4.1	15.1	54.1	63.8	18
Jul	5.3	10.4	94.4	55.1	58.9	6.9
Aug	4.5	10.8	140.3	55.4	57.1	3.1
Sep	4.3	8.2	90.2	42.4	46.2	9

5.1.2 Trends

The linear regression and the Sen's slope trend tests are used together with the bootstrapping and Mann-Kendall significance-testing methods, respectively, to compare the trends over the period 1960-2000 in yearly mean extreme precipitation and the yearly number of extreme precipitation events between the APHRODITE observations and the NorESM Historical 1 simulation. The relative trends are calculated taking the mean over the relation between each yearly value relative to the climatological mean. The results are presented in Table 5.3 and 5.4. For both the yearly extreme precipitation intensity and the yearly number of extreme events, the values are not significantly different between the observations and estimates. The relative trend in yearly extreme intensity show good agreement between the observed and simulated values for both regions and for both of the statistical methods. For the yearly number of extreme events, however, Krishna has too strong relative trends compared to the observations, while Godavari shows a too weak relative trend for the linear regression calculation, and a too strong relative trend for the Sen's slope.

Table 5.3: Trends and relative trends in the yearly mean daily extreme precipitation intensity over the period 1960-2000, retrieved from the APHRODITE observations and the NorESM Historical1 simulation (in parenthesis). Linear regression analysis and the Sen's slope are different statistical methods used to calculate trends, where the relative trend is calculated taking the mean over the relation between each yearly value relative to the climatological mean. CI_{min} and CI_{max} are the lower and upper 5 % significance level for the trends within the 99.5 percentile, and are calculated using the bootstrap method and the Mann-Kendall trend test along with the linear regression and the Sen's slope, respectively.

Region:	**Linear regression**	**CI_{min} lin. regression**	**CI_{max} lin. regression**	**Sen's slope**	**CI_{min} Sen's slope**	**CI_{max} Sen's slope**
Trend [mm/(1960-2000 period)]:						
Godavari	1.4 (-0.3)	-1.4 (-0.9)	4.1 (0.2)	2.3 (-0.4)	-0.9 (-1)	4.6 (0.3)
Krishna	0.3 (0)	-2.1 (-0.5)	2.7 (0.5)	0.4 (-0.1)	-2.1 (-0.6)	2.8 (0.4)
Relative trend [%]:						
Godavari	1.8 (-2.1)	-1.9 (-6.1)	5.6 (1.5)	3.0 (-2.7)	-1.2 (-6.8)	6.1 (1.7)
Krishna	0.6 (0.3)	-4.0 (-3.3)	4.7 (3.9)	0.8 (-0.5)	-3.9 (-3.9)	5.0 (2.6)

Table 5.4: Trends and relative trends in the yearly number of daily extreme precipitation events over the period 1960-2000 from the APHRODITE observations and the NorESM Historical1 simulation (in parenthesis). Linear regression analysis and the Sen's slope are different statistical methods to calculate trends, where the relative trend is calculated taking the mean over the relation between each yearly value relative to the climatological mean. CI_{min} and CI_{max} are the lower and upper 5 % significance level for the trends within the 99.5 percentile, and are calculated using the bootstrap method and the Mann-Kendall trend test along with the linear regression and the Sen's slope, respectively.

Region:	**Linear regression**	**CI_{min} lin. regression**	**CI_{max} lin. regression**	**Sen's slope**	**CI_{min} Sen's slope**	**CI_{max} Sen's slope**
Trend [no events/(1960-2000 period)]:						
Godavari	-1.8 (-0.1)	-3.1 (-0.8)	-0.6 (0.5)	-1.8 (-0.3)	-3.3 (-0.9)	0 (0)
Krishna	-1.6 (-0.6)	-3.6 (-1.1)	0.4 (-0.1)	-2.4 (-0.6)	-4.5 (-1.1)	0 (0)
Relative trend [%]:						
Godavari	-12.1 (-5.4)	-20.6 (-29.1)	-4.2 (17.8)	-11.6 (-12.7)	-21.9 (-32.4)	0 (0)
Krishna	-8.7 (-20.7)	-19.0 (-39.8)	1.4 (-1.5)	-13.1 (-21)	-24.6 (-39.6)	0 (0)

5.2. VERTICAL VELOCITY

The vertical velocity is not a given value in the NorESM dataset. Therefore, it has to be calculated using given values of horizontal winds, pressure and temperature through equations 2.12 - 2.15. To validate the vertical velocity during the monsoon months (June-September), the first task is to find out if adding the terrain-induced ω-term (last term in Equation 2.14) will improve the results. To test the quality of the calculated vertical velocity the reanalysed vertical velocity from NCEP1 is compared to calculations of vertical velocity (see eq. 2.12-2.15) with and without topography over the years 1960-1965 using reanalysed values of horizontal winds, pressure and temperature. The best-fit topography term is found for γ=1.9. Taking the 6-hourly area averaged vertical velocity within each catchment, the correlation between the reanalysed and the calculated vertical velocity (with and without topography) is calculated for each pressure level. The mean absolute percentage error (eq. 3.16) is also calculated for each of the calculated vertical velocities (with and without topography induced velocities). The calculation method with the highest correlations and the lowest mean absolute percentage error is selected for the calculation of vertical velocities in the NorESM simulations in the second part of validation and in the further investigations.

For both regions, the correlation between the reanalysis omega and the calculations are very similar regardless if the topography is included or not. Both Godavari and Krishna shows high correlations between 700-200 hPa, with values of ~0.8-0.9 and ~0.7-0.8, respectively (Figure 5.2). Regarding the mean absolute percentage error, the calculations with and without the topography term gives approximately equal results (Table 5.5 and 5.6), but the calculation of vertical velocity excluding topography shows slightly lower values and will be the preferred method through the thesis.

Next, we compare 6-hourly NorESM calculated vertical velocity values to the reanalysed NCEP1 vertical velocity over the whole period of interest (1960-2000). This is again done in two parts: As the main interest for precipitation are times with upward velocities, the vertical velocity-data with upward velocities ($\omega < 0$) is collected within each catchment, including only the pressure levels common for both datasets (925, 850, 700, 600, 500, 300, 250, 200, 150 and 100 hPa). Then the mean over the times with upward velocities is calculated, leaving us with a mean upward velocity value for each pressure level. This is performed for both the NCEP1 and NorESM datasets, thus allowing us to compare the vertical velocities in each pressure level. The same procedure is repeated for upward values of vertical velocity during the extreme precipitation events, which are selected using the NCEP1 reanalysed 99.5 percentile precipitation and the 6-hourly NorESM 99.5 percentile precipitation estimates.

When comparing NorESM to NCEP1 data, the vertical velocity at the mean days (Fig. 5.3, a and c) is overestimated in NorESM by about 40 % for Godavari and 60 % for Krishna between 500-300 hPa. For the levels below 700 hPa the vertical velocity is modelled too low. For the extreme days, the vertical velocity in NorESM is overestimated over the complete vertical profile for both regions (Fig. 5.3, b and d). Near the top and bottom, the difference is close to zero while it has its maximum at 500 hPa. Please note, that as observed in Figure 5.3, the NCEP1-vertical velocity values are very similar independent of using data from the mean or from the extreme events. This may be due to very low extreme precipitation values in the NCEP1 dataset, and thus the selection of extreme dates may not be coinciding with the highest amounts of vertical velocity. This also affects the specific humidity, the horizontal winds, and the temperature in Section 5.3 through 5.5.

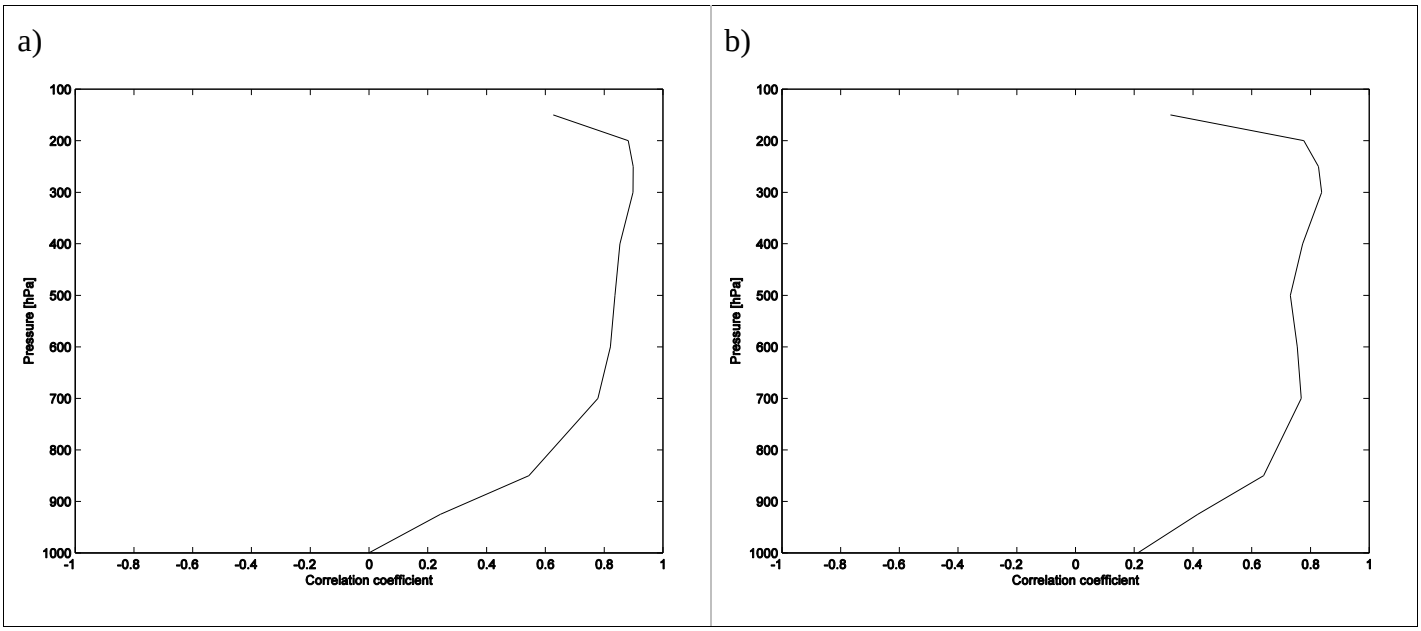

Figure 5.2: The correlation coefficients for each pressure level between 6-hourly NCEP1 reanalysed vertical velocity data and NCEP1 calculated vertical velocity data excluding topography (see Equation 2.13) for a) Godavari, and b) Krishna. The data is selected for the months June-September over the period 1960-1965.

Table 5.5: Mean absolute percentage error for Godavari between the 6-hourly NCEP1- and the NorESM Historical1 vertical velocity during the monsoon months (June-September) over the period 1960-1965.

Pressure level [hPa]:	Mean abs. error w/no topography [%]:	Mean abs. error w/topography [%]:
1000	18.1	19.5
925	4.3	4.6
850	23.5	23.3
700	8.2	8.4
600	0.6	0.4
500	2.5	2.1
400	2.1	2.4
300	6.1	6
250	0.2	0.5
200	7.9	7.9
150	6.8	6.8
100	2.7	1.8

Table 5.6: Mean absolute percentage error for Krishna between the 6-hourly NCEP1- and the NorESM Historical1 vertical velocity during the monsoon months (June-September) over the period 1960-1965.

Pressure level [hPa]:	Mean abs. error w/no topography [%]:	Mean abs. error w/topography [%]:
1000	9.9	10.9
925	56.5	57.3
850	21.5	21.9
700	2.4	2.5
600	1.3	1.5
500	8.5	8.5
400	0.2	0.3
300	7.8	7.5
250	6.5	6.6
200	14.2	14.2
150	18.2	18.1
100	17	18.4

The correlation between NCEP1 and NorESM Historical1 vertical velocity also shows similar results regardless of using mean- or extreme events data. However, Godavari has some larger agreement between them compared to Krishna. Krishna has a correlation of 0.74 for mean data against 0.76 for extreme data, while Godavari has 0.92 against 0.90, respectively.

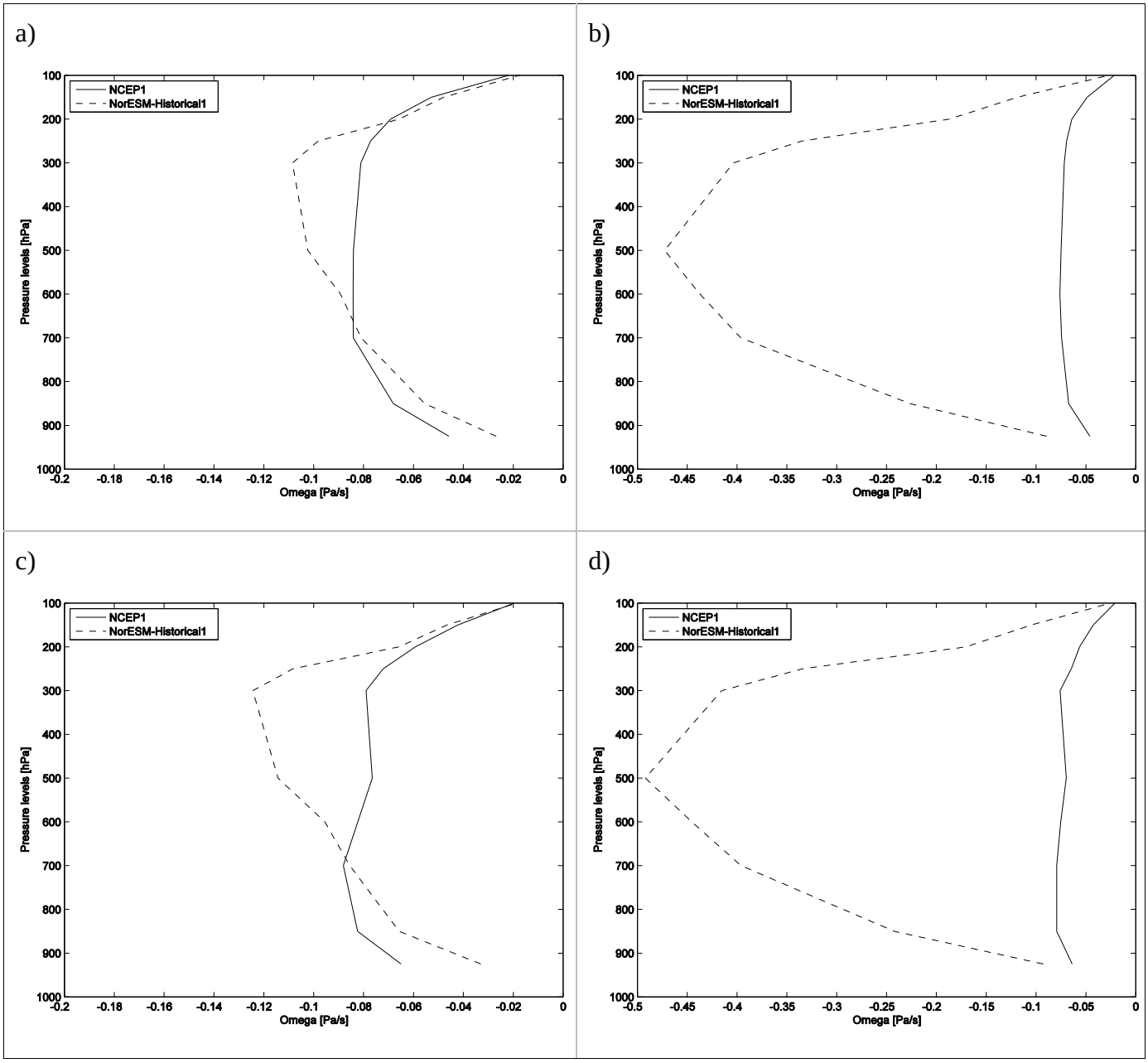

Figure 5.3: Monthly climatological mean (June-September) over the period 1960-2000 for upward vertical velocities (ω < 0). a) and b) are calculations for Godavari, and c) and d) are calculations for Krishna. Left column includes all data while the second column are for data during extreme precipitation events selected by NorESM - Historical1 simulation and the NCEP1 reanalysis.

5.3. INTEGRATED WATER VAPOUR TRANSPORT

The 6-hourly integrated water vapour transport is calculated using Equation 2.16 through 2.18, and both the mean and extreme data are investigated. To gain values during extreme events, dates defined by the 99.5 percentile of the 6-hourly NCEP1 reanalysis precipitation is used to select the horizontal winds and the specific humidity in the NCEP1 reanalysis. The same procedure is performed for the NorESM Historical1 data, except here the dates of the 99.5 percentile of the NorESM Historical1 precipitation is used to select each of the variables. The relative difference between the timely mean integrated water vapour transport calculated in NorESM and NCEP1 is calculated for both mean data and for data during extreme precipitation, with the bootstrapping technique used for significance testing. These results, in addition to the mean value per month for the each of the datasets, are presented in Table 5.7 and 5.8. It is worth noting that the data in "All months" is not calculated taking the mean over the monthly means, but by taking the mean over the unsorted data.

In general, the relative differences are smaller for the mean data than they are during extreme precipitation events. Considering all months, the mean data in Godavari is underestimated by 22 %, while the data during extreme events is significantly overestimated by 91%. The differences between the months show that the mean data has a range in the relative difference from -13 % for June to 47 % for September, with only August and September having significant results. The data during extreme events has significant values for all months, ranging from 47 to 203 %, where July and September are the months with the smallest and largest bias, respectively.

Table 5.7: Mean values and relative differences between 6-hourly NorESM Historical1 and NCEP1 calculated integrated water vapour transport for both mean data and for data during 99.5 percentile precipitation events over Godavari. Data covering June-September over the period 1960-2000 is used.

	NorESM – mean data [kg m^{-1} s^{-1}]:	**NCEP1 – mean data [kg m^{-1} s^{-1}]:**	**Relative difference [%]:**	**NorESM – 99.5 pctl prec. dates [kg m^{-1} s^{-1}]:**	**NCEP1 – 99.5 pctl prec. dates [kg m^{-1} s^{-1}]:**	**Relative difference [%]:**
Jun	213.2	245.5	-13.2	446.8	252.9	76.6
Jul	329.1	288.1	14.2	474	321.9	47.2
Aug	371.6	254.9	45.8	540.5	262.8	105.6
Sep	259.1	176.4	46.9	530	174.9	203
All months	**294.2**	**241.7**	**21.7**	**518.7**	**271.5**	**91**

For Krishna the biases are smaller than they are for Godavari. The integrated water vapour transport calculated for NorESM Historical1 and NCEP1 when including all months for the mean data show approximately equal amounts, and the relative difference thus equals zero although the solution is insignificant. The data during extreme precipitation events is simulated too large, and is significantly overestimated by 41 %. For the monthly mean data, June is significantly underestimated by 31 %, while the remaining months are overestimated between 3 and 16%, though either of them are significant. The data during extreme precipitation events ranges between 20 and 94 %, where only August and September have significantly larger values. This larger overestimation during extreme precipitation events compared to the mean data may again be due to the bad relationship between precipitation and the remaining variables in the NCEP1 reanalysis.

Table 5.8: Mean values and relative differences between 6-hourly NorESM Historical1 and NCEP1 calculated integrated water vapour transport for both mean data and for data during 99.5 percentile precipitation events over Krishna. Data covering June-September over the period 1960-2000 is used.

	NorESM – mean data [kg m^{-1} s^{-1}]:	**NCEP1 – mean data [kg m^{-1} s^{-1}]:**	**Relative difference [%]:**	**NorESM – 99.5 pctl prec. dates [kg m^{-1} s^{-1}]:**	**NCEP1 – 99.5 pctl prec. dates [kg m^{-1} s^{-1}]:**	**Relative difference [%]:**
Jun	239.8	345.7	-30.7	445.4	371.6	19.9
Jul	442.3	431.6	2.5	608.1	486.1	25.1
Aug	468.8	405.3	15.7	658.9	422.2	56.1
Sep	279.6	249.7	12	488.9	252.1	93.9
All months	**359.2**	**359.1**	**0**	**588.2**	**416.2**	**41.4**

5.4. DIVERGENCE

The horizontal divergence is calculated using Equation 2.19, and to calculate the mean vertical profile Equation 3.12 and 3.13 are used. Again, the 6-hourly NorESM Historical1 data is compared to the NCEP1 reanalysis data, and for the extreme events the 99.5 percentile precipitation times from each of the datasets are used. The differences and relative differences over the vertical profile are calculated taking the mean of Equation 3.14 and 3.15, respectively, and due to different pressure sections in the two data sets, only the common pressure levels (925, 850, 700, 600, 500, 300, 250, 200, 150 and 100 hPa) has been applied.

The bootstrapping technique (Section 3.3.2) is used to calculate the significance in the differences and relative differences between the two datasets.

For both regions, the validation of mean data shows better results than for the data during times of extreme precipitation. The differences between NorESM and NCEP1 for mean data are in the order of 10^{-6}-10^{-8} s^{-1}, while for the 99.5 percentile precipitation events they are approximately 10^{-5} -10^{-6} s^{-1} (see Figure 5.4 and 5.5, and Table 5.9 and 5.10). This larger deviation in the data during extreme precipitation dates are due to the error in extreme precipitation found in the NCEP1 data (see Section 5.2).

In general, both the convergence and divergence is overestimated/stronger in NorESM Historical1 compared to the NCEP1 data. This can explain the overestimation of the vertical velocity found in Section 5.2, as the two parameters are strongly connected (Equation 2.12).

Table 5.9: The 6-hourly mean divergence over Godavari during mean- and 99.5 percentile precipitation times for NorESM Historical1 and the NCEP1 data during the monsoon months over the period 1960-2000. In addition, the difference and relative difference in divergence between each of the datasets is presented.

Pressure levels [hPa]:	Mean div. NCEP1 [s^{-1}]:	Mean div. NorESM [s^{-1}]:	Difference mean div. [s^{-1}]:	Rel. difference mean div. [%]:	Divergence - 99.5 pctl prec. times, NCEP1 [s^{-1}]:	Divergence - 99.5 pctl prec. times, NorESM [s^{-1}]:	Difference divergence, 99.5 pctl prec. times [s^{-1}]:	Rel. difference divergence, 99.5 pctl prec. times [%]:
1000	-3.4E-06	-3.8E-06	-4.0E-07	12.5	-3.4E-06	-2.2E-05	-1.9E-05	589.8
925	-4.2E-06	-4.2E-06	5.3E-08	1.2	-4.1E-06	-3.1E-05	-2.7E-05	687.6
850	-2.3E-06	-1.2E-06	1.0E-06	-47.1	-2.7E-06	-1.6E-05	-1.3E-05	516.7
700	-1.3E-08	-6.1E-07	-5.9E-07	119	5.4E-07	-1.1E-05	-1.1E-05	662.7
600	5.8E-07	-2.8E-07	-8.6E-07	-174.1	9.4E-07	-6.9E-06	-7.9E-06	-1,894.9
400	6.5E-07	2.6E-07	-3.8E-07	-61.6	5.0E-07	-1.2E-06	-1.7E-06	544
300	6.9E-07	5.4E-07	-1.4E-07	- 5.6	5.5E-07	5.1E-06	4.5E-06	233.2
250	8.9E-07	8.5E-07	-3.2E-08	9.8	8.8E-07	1.8E-05	1.7E-05	77.1
200	2.4E-07	1.3E-06	1.1E-06	592.9	-2.4E-07	2.3E-05	2.4E-05	7,282.8
150	7.6E-08	4.8E-06	4.7E-06	1,511.7	-5.2E-07	3.4E-05	3.5E-05	14,926

Table 5.10: The 6-hourly mean divergence over Krishna during mean- and 99.5 percentile precipitation times for NorESM Historical1 and the NCEP1 data during the monsoon months over the period 1960-2000. In addition, the difference and relative difference in divergence between each of the datasets is presented.

Pressure levels [hPa]:	Mean div. NCEP1 [s^{-1}]:	Mean div. NorESM [s^{-1}]:	Difference mean div. [s^{-1}]:	Rel. difference mean div. [%]:	Divergence - 99.5 pctl prec. times, NCEP1 [s^{-1}]:	Divergence - 99.5 pctl prec. times, NorESM [s^{-1}]:	Difference divergence, 99.5 pctl prec. times [s^{-1}]:	Rel. difference divergence, 99.5 pctl prec. times [%]:
1000	-1.4E-06	-4.5E-06	-3.1E-06	-241.7	-1.3E-06	-1.7E-05	-1.6E-05	-1,412
925	-8.7E-07	-3.9E-06	-3.0E-06	-419.3	-5.0E-07	-2.2E-05	-2.1E-05	-5,662.5
850	-1.8E-06	-6.2E-07	1.2E-06	67.8	-1.4E-06	-1.8E-05	-1.7E-05	-1,440.7
700	3.8E-07	5.2E-07	1.4E-07	-677.2	7.6E-07	-9.3E-06	-1.0E-05	-2,029.7
600	5.7E-07	-3.9E-07	-9.5E-07	-162.6	4.4E-07	-6.1E-06	-6.6E-06	-2,222.7
400	-6.7E-08	-3.6E-07	-3.0E-07	-269.7	-5.6E-07	-2.2E-06	-1.7E-06	-263.3
300	6.7E-07	3.5E-07	-3.2E-07	-47.8	7.3E-07	5.0E-06	4.3E-06	470.1
250	1.6E-06	1.7E-06	1.3E-07	4.3	1.4E-06	2.0E-05	1.9E-05	1068.1
200	1.4E-06	2.4E-06	1.1E-06	119.3	8.9E-07	2.6E-05	2.5E-05	2722.6
150	7.6E-07	4.9E-06	4.2E-06	358.4	9.6E-07	2.8E-05	2.7E-05	2787.1

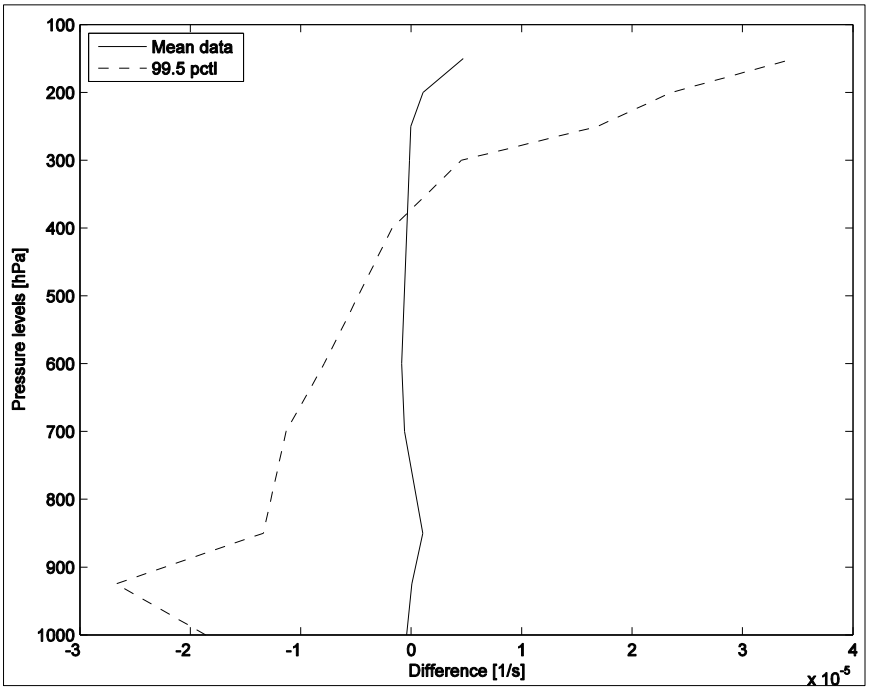

Figure 5.4: Validation profiles of mean horizontal divergence over Godavari showing the difference between 6-hourly NorESM Historical1 and NCEP1 data during monsoon months over the period 1960-2000. The extreme data in NorESM and NCEP1 is selected at the times of the 99.5 percentile precipitation from the NorESM simulation and NCEP1 reanalysis, respectively.

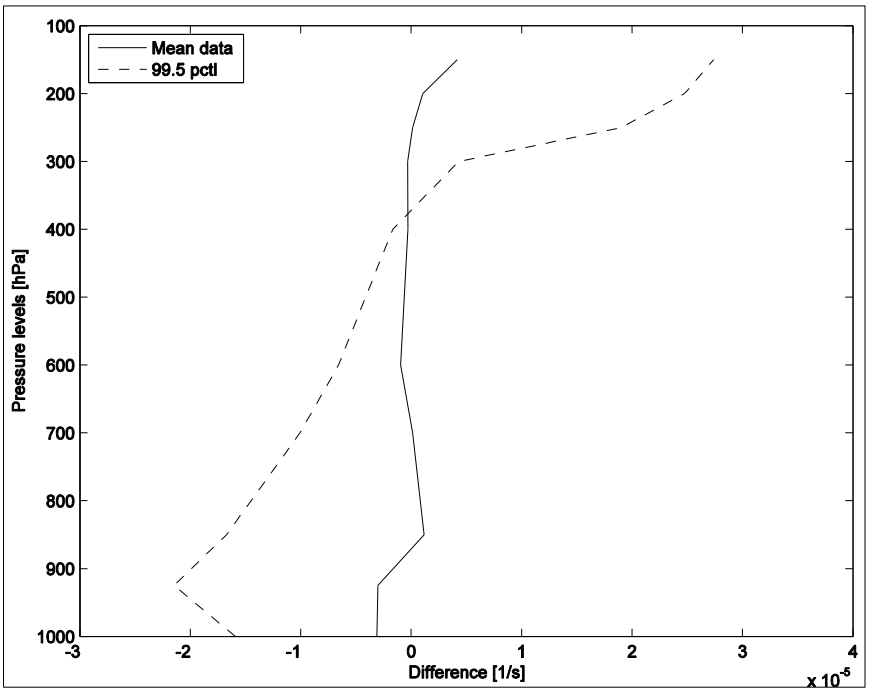

Figure 5.5: Validation profiles of mean horizontal divergence over Krishna showing the difference between 6-hourly NorESM Historical1 and NCEP1 data during monsoon months over the period 1960-2000. The extreme data in NorESM and NCEP1 is selected at the times of the 99.5 percentile precipitation from the NorESM simulation and NCEP1 reanalysis, respectively.

5.5. TEMPERATURE

The validation of temperature is performed comparing the 6-hourly mean temperature profile over the period 1960-2000 for the NorESM data with the 6-hourly NCEP1 reanalysis temperature for each catchment. In addition, the mean temperature profiles during the 99.5 percentile precipitation times in each of the datasets are compared (see Section 3.4.2 for equations). As for the vertical velocity and the horizontal divergence, only the common pressure levels (925, 850, 700, 600, 500, 300, 250, 200, 150 and 100 hPa) are included in the calculations. The results are presented in Table 5.11 and 5.12, and the differences in Figure 5.6 and 5.7.

From Figure 5.6 and 5.7 it is observable that the largest errors over the profile is found for the temperature during the 99.5 percentile precipitation events. For both regions, the largest relative difference is found at the 600 hPa layer. Here the mean data of the NorESM data is estimated to be approximately 110 % overestimated, with a mean value of 8 °C (NorESM) compared to 4 °C (NCEP1), and the data during 99.5 percentile precipitation events is significantly overestimated by 95-96 %, depending on the region. The smallest bias is on the other hand found between 850-925 hPa and 200-250 hPa.

The mean temperature of the NCEP1 reanalysis in Table 5.11 and 5.12 is the same for both mean precipitation events as during events within the 99.5 percentile precipitation. This is due to the error in extreme precipitation found in the NCEP1 data (see Section 5.2).

Table 5.11: The 6-hourly mean temperature over Godavari during mean- and 99.5 percentile precipitation times for NorESM and the NCEP1 data during the monsoon months over the period 1960-2000. In addition, the difference and relative difference in temperature between each of the datasets is presented.

Pressure level [hPa]:	Mean temp., NCEP1 [°C]:	Mean temp., NorESM [°C]:	Difference mean temp. [°C]:	Rel. difference mean temp. [%]:	Temp. - 99.5 pctl prec. times, NCEP1 [°C]:	Temp. - 99.5 pctl prec. times, NorESM [°C]:	Difference temp., 99.5 pctl prec. times [°C]:	Rel. difference temp., 99.5 pctl prec. times [%]:
1000	28.3	26.3	**-2.0**	**-6.8**	28.2	23.6	**-4.6**	**-15.5**
925	24.3	25.2	**0.9**	**3.9**	24.3	22.8	**-1.5**	**-5.5**
850	19.7	18.9	**-0.9**	**-4.3**	19.8	18.4	**-1.4**	**-6.4**
700	10.5	14.0	**3.6**	**34.1**	10.5	14.2	**3.7**	**35.2**
600	4.3	8.6	**4.3**	**107.4**	4.3	8.1	**3.8**	**95.9**
400	-12.8	-11.8	**1**	**8.1**	-12.7	-10.3	**2.5**	**19.4**
300	-26.6	-20	**6.7**	**25.0**	-26.5	-17.4	**9.0**	**34.1**
250	-36.5	-38.0	**-1.5**	**-4.1**	-36.4	-35.1	**1.4**	**3.7**
200	-48.1	-47.0	**1**	**2.1**	-48.1	-44.9	**3.2**	**6.7**
150	-62.8	-71.2	**-8.4**	**-13.4**	-62.7	-72.0	**-9.3**	**-14.8**

Table 5.12: The 6-hourly mean temperature over Krishna during mean- and 99.5 percentile precipitation times for NorESM and the NCEP1 data during the monsoon months over the period 1960-2000. In addition, the difference and relative difference in temperature between each of the datasets is presented.

Pressure level [hPa]:	Mean temp., NCEP1 [°C]:	Mean temp., NorESM [°C]:	Difference mean temp. [°C]:	Rel. difference mean temp. [%]:	Temp. - 99.5 pctl prec. times, NCEP1 [°C]:	Temp. - 99.5 pctl prec. times, NorESM [°C]:	Difference temp., 99.5 pctl prec. times [°C]:	Rel. difference temp., 99.5 pctl prec. times [%]:
1000	27.5	25.0	**-2.5**	**-9**	27.2	22.3	**-4.9**	**-17.9**
925	23.5	23.8	**0.3**	**1.3**	23.2	21.3	**-1.9**	**-7.9**
850	18.8	17.6	**-1.1**	**-5.9**	18.6	16.7	**-1.9**	**-9.9**
700	9.9	13.1	**3.2**	**31.9**	10.0	12.9	**2.9**	**29**
600	3.7	7.8	**4.1**	**111.9**	3.6	7.0	**3.4**	**92.6**
400	-13.7	-12.4	**1.2**	**9.1**	-13.7	-10.5	**3.2**	**23.2**
300	-27.7	-20.5	**7.1**	**25.7**	-27.6	-17.6	**10.0**	**36.2**
250	-37.4	-38.7	**-1.2**	**-3.3**	-37.5	-34.7	**2.8**	**7.2**
200	-49.1	-47.8	**1.3**	**2.6**	-49.1	-44.2	**5.0**	**10**
150	-63.8	-71.9	**-8.1**	**-12.7**	-63.7	-69.9	**-6.2**	**-9.7**

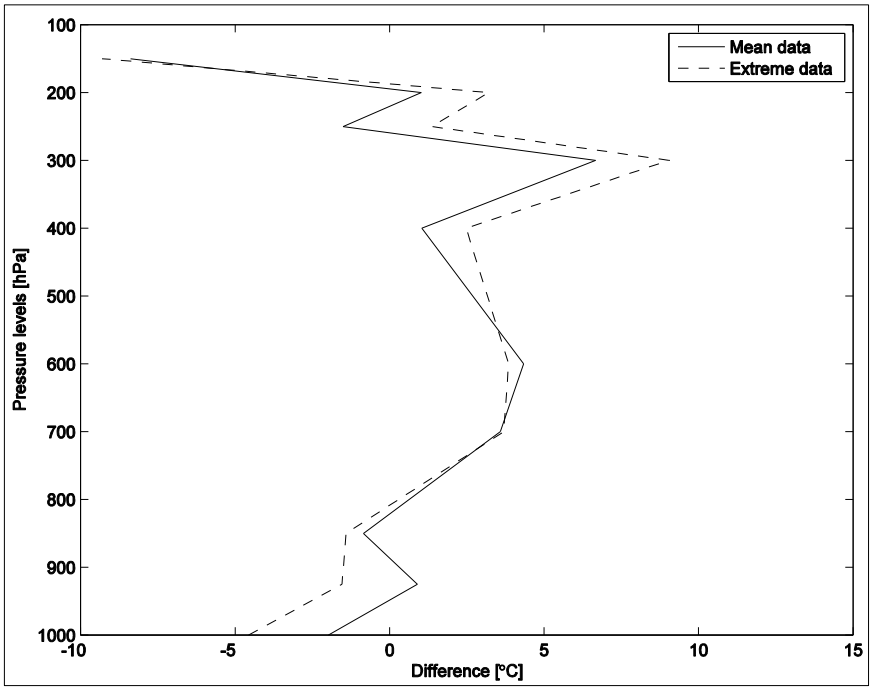

Figure 5.6: Validation profiles of the mean temperature over Godavari showing the difference between 6-hourly NorESM Historical1 and NCEP1 data during monsoon months over the period 1960-2000. The extreme data in NorESM and NCEP1 is selected at the times of the 99.5 percentile precipitation from the NorESM Historical1 simulation and NCEP1 reanalysis, respectively.

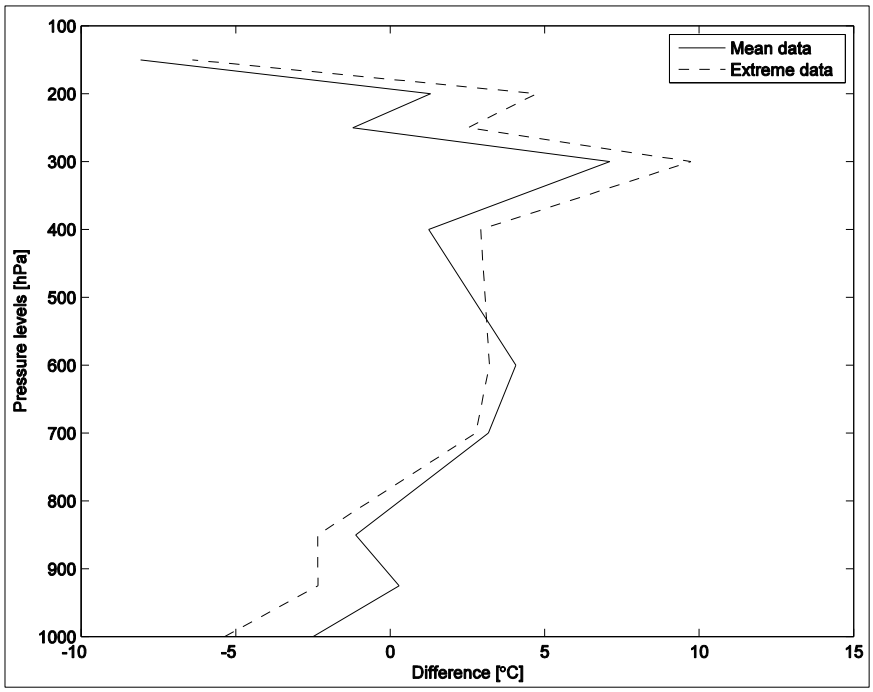

Figure 5.7: Validation profiles of the mean temperature over Krishna showing the difference between 6-hourly NorESM Historical1 and NCEP1 data during monsoon months over the period 1960-2000. The extreme data in NorESM and NCEP1 is selected at the times of the 99.5 percentile precipitation from the NorESM Historical1 simulation and NCEP1 reanalysis, respectively.

6. Results

This chapter presents the precipitation simulated by the NorESM in both historic and future perspectives, in addition to calculations of vertical velocity, divergence, water vapour transport and convective available potential energy. The purpose is to connect all the variables to find which of them are more important in the generation of extreme precipitation.

6.1. 6-HOURLY EXTREME PRECIPITATION EVENTS

6.1.1. NorESM Historical1 simulation

In accordance with the observations the NorESM has most of the precipitation in the catchments Godavari and Krishna occurring during the monsoonal months June-September (see Figure 6.1). The highest mean amounts are found in August (657 mm) and September (492 mm), with the amounts in August being more than twice the value of July (248 mm). The comparison to observations can be found in Table 5.1 and 5.2.

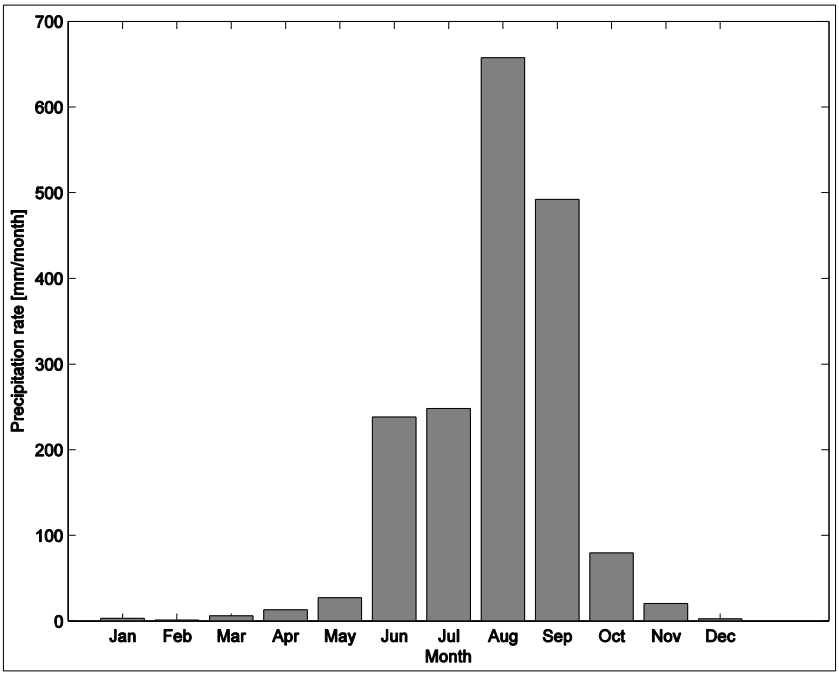

Figure 6.1: Average precipitation rate per month over the period 1960-2000 for the regions Godavari and Krishna. The data is taken from NorESMs' Historical1 6-hourly simulation.

When studying the intensity of the extreme events (defined as the 6-hourly events exceeding the 99.5 percentile over the period 1960-2000) there is a small difference between the selected months (Figure 6.2 and 6.3). August is the month with slightly higher intensity and the

highest number of extreme days, while June has the fewest number of extreme events. For June, July and September the mean intensity is approximately the same (~32 mm/6hr).

To what extent the NorESM is under or overestimating 6-hourly extremes is not known, as there are no observed 6-hourly precipitation to compare against. However, the validation of the daily data in Section 5.1 indicates that the model is underestimating the extremes in Godavari while the results for Krishna was satisfactory (Table 5.1 and 5.2).

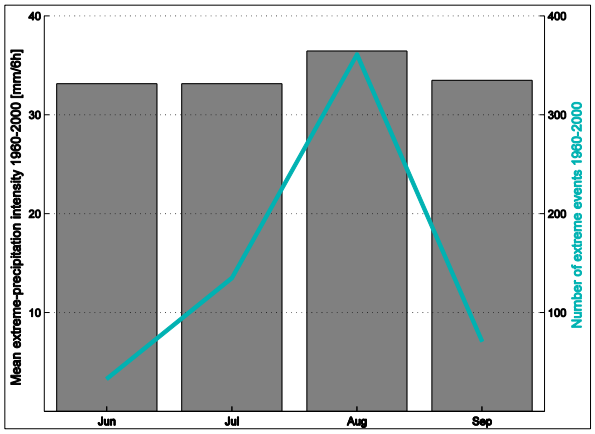

Figure 6.2: Mean intensity of 6-hourly extreme precipitation (bars) and total number of extreme events (line) over the years 1960-2000 for Godavari. The data is retrieved from the NorESM Historical1 simulation.

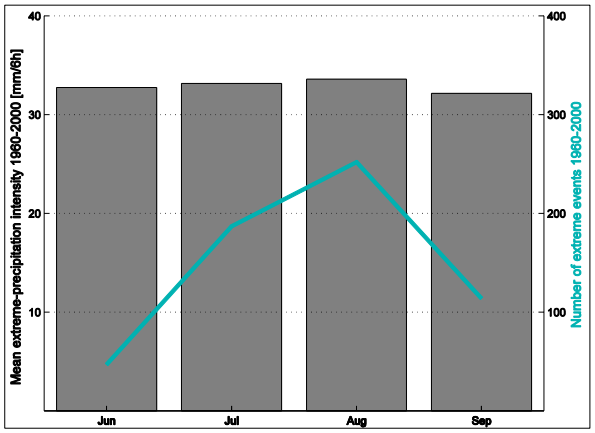

Figure 6.3: Mean intensity of 6-hourly extreme precipitation (bars) and total number of extreme events (line) over the years 1960-2000 for Krishna. The data is retrieved from the NorESM Historical1 simulation.

The change in yearly mean extreme precipitation amounts and in the yearly number of extreme precipitation events over the period 1960-2000 is calculated using both linear regression analysis (Section 3.1) and by calculating the Sen's slope (Section 3.2). The significance is tested using the bootstrapping method (Section 3.3.2) together with the linear regression trend data, and by using the Mann-Kendall trend test (Section 3.3.1) along with the Sen's slope trend data. The relative trends are calculated taking the mean over the relation between each yearly value relative to the climatological mean.

A decrease in the number of extreme precipitation events per year is detected, but the trend is not significant (Table 6.2). For Godavari the trend has a decrease of approximately 1-2 events over the period while Krishna has a decrease of 1 event, or equivalently a decrease of 6-16 % and 11 %, respectively, depending on the applied statistical method. For the yearly mean precipitation intensity, there is an insignificant decrease of approximately 1 mm (~2 %) per event for Godavari, while Krishna shows nearly no decrease at all (~0.5 mm, Table 6.1).

Table 6.1: Trends and relative trends in the yearly mean 6-hourly extreme precipitation intensity over the period 1960-2000, retrieved from the NorESM Historical1 simulation. Linear regression analysis and the Sen's slope are different statistical methods used to calculate trends, where the relative trend is calculated taking the mean over the relation between each yearly value relative to the climatological mean. CI_{min} and CI_{max} are the lower and upper 5 % significance level for the trends within the 99.5 percentile, and are calculated using the bootstrap method and the Mann-Kendall trend test along with the linear regression and the Sen's slope, respectively.

Region:	Linear regression	CI_{min} lin. regression	CI_{max} lin. regression	Sen's slope	CI_{min} Sen's slope	CI_{max} Sen's slope
Trend [mm/(1960-2000 period)]:						
Godavari	-0.6	-1.3	0.2	-0.8	-1.6	0
Krishna	-0.2	-1.0	0.5	-0.5	-1.3	0.1
Relative trend [%]:						
Godavari	-1.7	-3.9	0.6	-2.4	-4.7	0
Krishna	-0.8	-3.3	1.6	-1.5	-4.0	0.3

Table 6.2: Trends and relative trends in the yearly number of 6-hourly extreme precipitation events over the period 1960-2000 from the NorESM Historical1 simulation. Linear regression analysis and the Sen's slope are different statistical methods to calculate trends, where the relative trend is calculated taking the mean over the relation between each yearly value relative to the climatological mean. CI_{min} and CI_{max} are the lower and upper 5 % significance level for the trends within the 99.5 percentile, and are calculated using the bootstrap method and the Mann-Kendall trend test along with the linear regression and the Sen's slope, respectively.

Region:	Linear regression	CI_{min} lin. regression	CI_{max} lin. regression	Sen's slope	CI_{min} Sen's slope	CI_{max} Sen's slope
Trend [no events/(1960-2000 period)]:						
Godavari	-0.7	-2.9	1.6	-1.7	-3.3	0.4
Krishna	-1.2	-3.0	0.7	-1.3	-3.3	0.8
Relative trend [%]:						
Godavari	-6.0	-25.8	13.7	-15.7	-30.1	3.6
Krishna	-10.5	-27.0	5.3	-11.2	-29.1	6.7

6.1.2. RCP8.5

The relative change in number of extreme events and in the mean extreme precipitation intensity between the NorESM RCP8.5 scenario for the period 2060-2100 and the NorESM Historical1 simulation for the period 1960-2000 is calculated. Both the historic and future number of extreme dates is calculated by counting the number of events above a threshold value selected by using percentiles based on the historic data. For the extreme precipitation intensity, the historic extreme values are selected relative to a historic extreme threshold,

while the future extreme values are selected relative to a future extreme threshold. Then the timely mean is calculated for both the historic and the future values, before taking the mean of the relative difference between them. Four different time-steps have been compared; 6-hour, daily, 10-days and monthly data. In addition, all the calculations are applied to the 95, 99, and the 99.5 percentiles. The results are presented in Table 6.3 and 6.4.

There are significant increases in both the number of extreme days and in the mean extreme precipitation intensity between the two periods (see Figure 6.4 and 6.5). The only exception is in the 6-hourly 95 percentile where Godavari has a significant decrease of -22 % and Krishna has an insignificant decrease of -5%. For the 6-hourly 99.5 percentile data, the number of days increases with 42 % for Godavari, while the values nearly doubles for Krishna with a 95 % increase. For the change in mean extreme precipitation intensity the values rises with 30 % and 34 % in Godavari and Krishna, respectively. Between the two regions, Krishna has a larger change than Godavari does for all percentiles and time-periods, except for the 10-day change in the mean extreme precipitation data in the 99 and 99.5 percentile.

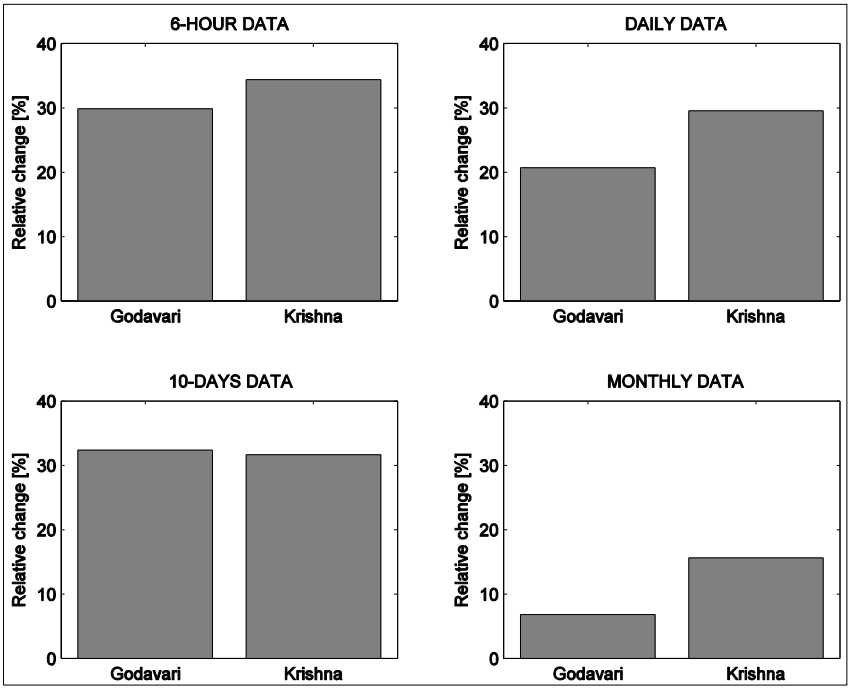

Figure 6.4: Relative change in the mean extreme precipitation intensity between the RCP8.5 scenario over the period 2060-2100 and the Historical1 simulation over the period 1960-2000 for the 99.5 percentile.

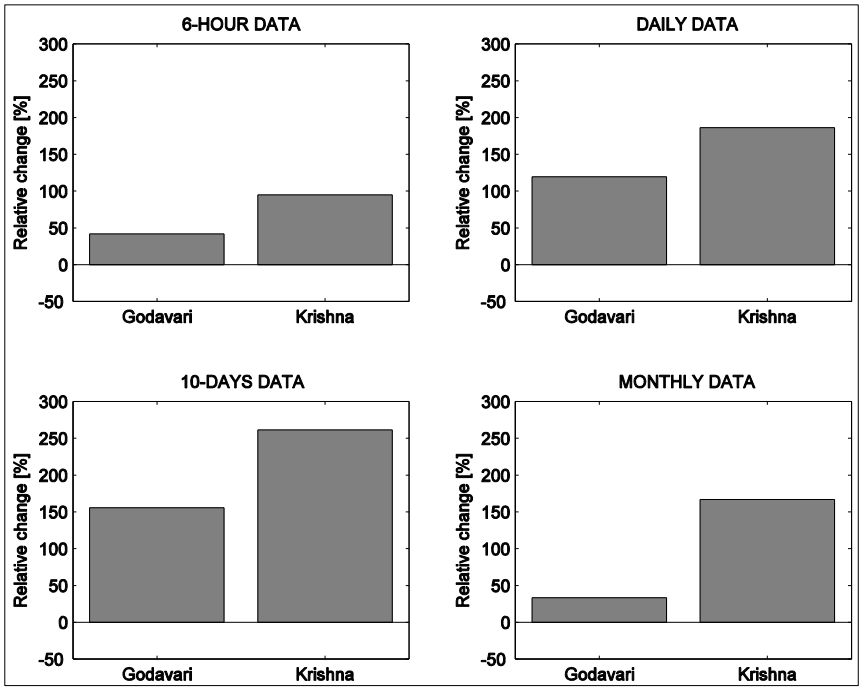

Figure 6.5: Relative change in the number of extreme precipitation events between the RCP8.5 scenario over the period 2060-2100 and the Historical1 simulation over the period 1960-2000 for the 99.5 percentile.

It is interesting to study how the relative change in the number of extreme events and in the mean extreme precipitation intensity depends on the percentiles. For the 6-hourly data, there are small differences between relative changes in the 95, 99 and 99.5 percentiles, but they tend to increase with percentile. However, for the 97.5 and 98.5 percentiles, the relative changes drops to approximately half the value of the 95 and 99 percentiles (see Figure 6.6 and 6.7), and the same is observed from the 99.5 to the 99.9 percentile for the change in the mean extreme precipitation. The monthly data is the only period in which the relative change decreases as the events become more extreme (Table 6.3 and 6.4).

In general, for all time distributions except the monthly data, the relative change between the future and historic data in both the mean extreme intensity and in the number of extreme events in the 99.5 percentile increases with increasing time step. From the 10-day period to the monthly period the relative difference decreases sharply.

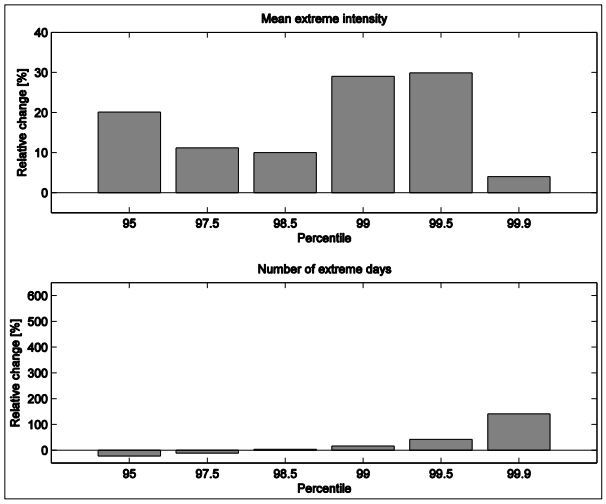

Figure 6.6: Relative change between the NorESM RCP8.5 scenario over the period 2060-2100 and the NorESM Historical1 simulation over the period 1960-2000 in mean extreme precipitation intensity (top) and in the number of extreme precipitation events (bottom) for the 6-hourly data in Godavari.

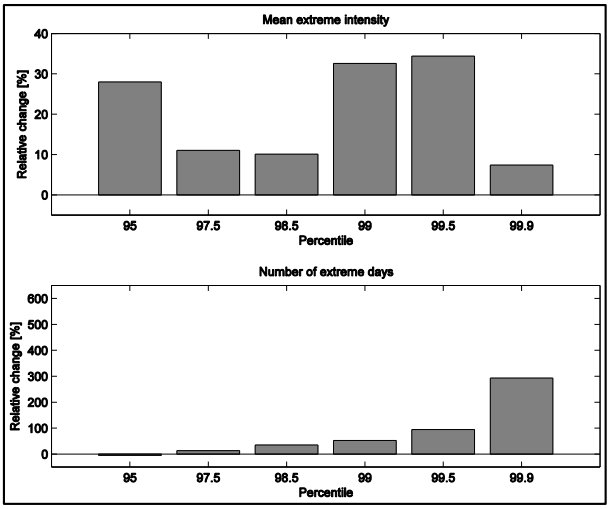

Figure 6.7: Relative change between the NorESM RCP8.5 scenario over the period 2060-2100 and the NorESM Historical1 simulation over the period 1960-2000 in mean extreme precipitation intensity (top) and in the number of extreme precipitation events (bottom) for the 6-hourly data in Krishna.

Table 6.3: The relative change in 6-hourly extreme precipitation intensity between the NorESM RCP8.5 scenario over the period 2060-2100 and the NorESM Historical1 simulation over the period 1960-2000. Four different time-distributions and three different percentiles are presented. CI_{min} and CI_{max} are the lower and upper limits for the trends within the 5 % significance level, respectively, and forms the confidence interval (CI).

	95 pctl			**99 pctl**			**99.5 pctl**		
Region	**Rel. difference [%]:**	**CI_{min} [%]:**	**CI_{max} [%]:**	**Rel. difference [%]:**	**CI_{min} [%]:**	**CI_{max} [%]:**	**Rel. difference [%]:**	**CI_{min} [%]:**	**CI_{max} [%]:**
6-hour									
Godavari	20.1	9.5	32.7	29	17.2	42.7	29.9	18.4	43.5
Krishna	28	18.2	39.3	32.6	22.9	44.1	34.4	23.4	48.3
Daily									
Godavari	17	8.6	28.1	21.4	10.5	35.1	20.7	9.2	35.7
Krishna	21.7	11	34.7	26.1	14.3	41.6	29.6	16.5	46.6
10-Days									
Godavari	17.6	8.4	28.1	28	14.3	44.4	32.4	16.9	49.1
Krishna	22.9	7.3	44	25.6	7.5	51	31.6	11.2	62.3
Monthly									
Godavari	11	0.5	25.2	9.2	-4.2	26.4	6.8	-8.9	24.7
Krishna	18.4	2.9	38.3	16.6	2.5	36	15.6	0.9	36.4

Table 6.4: The relative change in the number of 6-hourly extreme precipitation events between the NorESM RCP8.5 scenario over the period 2060-2100 and the NorESM Historical1 simulation over the period 1960-2000. Four different time-distributions and three different percentiles are presented. CI_{min} and CI_{max} are the lower and upper limits for the trends within a 5 % significance level, respectively, and forms the confidence interval (CI).

	95 pctl			99 pctl			99.5 pctl		
Region	**Rel. difference [%]:**	**CI_{min} [%]:**	**CI_{max} [%]:**	**Rel. difference [%]:**	**CI_{min} [%]:**	**CI_{max} [%]:**	**Rel. difference [%]:**	**CI_{min} [%]:**	**CI_{max} [%]:**
6hour									
Godavari	-22.3	-31	-13.1	15.8	6.8	24.9	41.8	28.3	55.3
Krishna	-5.3	-15	3.1	52.2	30	68.5	94.8	59.7	122.1
Daily									
Godavari	30.6	19.1	39.7	82.7	70	96.3	119.3	105.3	133.3
Krishna	47.7	34.6	61.3	122.3	84.7	157.3	186	123.3	238.7
10-Days									
Godavari	60.7	26.7	96	116.7	83.3	146.7	155.6	100	222.2
Krishna	129.3	101.3	159.3	283.3	203.3	363.3	261.1	122.2	405.6
Monthly									
Godavari	83.3	56.3	112.5	75	8.3	175	33.3	-50	116.7
Krishna	131.3	85.4	181.3	216.7	66.7	375	166.7	133.3	200

6.2. INTEGRATED WATER VAPOR TRANSPORT AND DIVERGENCE

The horizontal divergence profile and integrated water vapour transport is calculated using 6-hourly data from the NorESM Historical1 simulation and the NorESM RCP8.5 scenario. The extreme data is selected at the times of the 99.5 percentile precipitation during the monsoon months over the periods 1960-2000 (historical) and 2060-2100 (future). The divergence is calculated using Equation 2.19, while the water vapour transport is calculated using Equation 2.16-2.18, where the upper level of the atmosphere is set to 100 hPa. The calculations of divergence are time and area averaged, leaving a vector with one value per pressure level, while the integrated water vapour transport only are time averaged.

For the divergence profile, the difference between values on extreme and mean precipitation events is calculated for both future and historic values, as well as the difference between future and historic values on extreme and mean precipitation days. The vertical profiles for Godavari and Krishna are presented in Figure 6.8 and 6.10,

respectively, and their differences in Figure 6.9 and 6.11. In Table 6.5 and 6.6 the relative differences within the mean divergence and convergence over the atmospheric column is presented, and by using the bootstrap method they are all found to be statistically significant.

The divergence profiles show maximum convergence at approximately 950 hPa and maximum divergence at 150 hPa, with the transition from convergence to divergence in Krishna occurring at approximately 400 hPa for the historic and future mean data, and at approximately 300 hPa during historic and future extreme precipitation events. For Godavari the transition is lower towards the ground; at 470 hPa for historic and future mean data, and at 400 hPa for historic and future extreme precipitation events.

Despite the fact that the convergence occurs over a larger portion of the atmosphere than the divergence, the total amount of divergence over the profile is stronger with approximately 250 % larger values. Over Krishna, this relationship will stay approximately constant in the future for both mean data and for data on extreme precipitation events, as both the divergence and convergence will decrease with ~13-14 % in the mean data and increase with 42-44 % during extreme precipitation events, respectively (Table 6.6). In Godavari, the relationship will decrease for the mean data in the future as the divergence decreases by 20 % and the convergence by 16 %, while for the extreme precipitation events, the difference will stay more or less constant, as the convergence and divergence will increase by 4 % and 3 %, respectively (Table 6.5).

Table 6.5: The relative differences between the future (2060-2100) and historic (1960-2000) values, and between data during events with extreme precipitation (99.5 pctl) and mean data, in 6-hourly mean convergence and divergence over Godavari is presented. The Historical1 simulation and the RCP8,5 scenario of the NorESM data has been used in the calculation. All data are significant.

	Rel. difference, RCP8.5-Historical1, mean data [%]:	**Rel. difference, RCP8.5-Historical1, 99.5 pctl [%]:**	**Rel. difference, 99.5 pctl-mean data, Historical1 [%]:**	**Rel. difference, 99.5 pctl-mean data, RCP8.5 [%]:**
Mean convergence	-15.6	4.2	1056.6	1291.9
Mean divergence	-19.5	3.2	941.7	1224.2

Table 6.6: The relative differences between the future (2060-2100) and historic (1960-2000) values, and between data during events with extreme precipitation (99.5 pctl) and mean data, in 6-hourly mean convergence and divergence over Krishna is presented. The Historical1 simulation and the RCP8,5 scenario of the NorESM data has been used in the calculation. All data are significant.

	Rel. difference, RCP8.5-Historical1, mean data [%]:	**Rel. difference, RCP8.5-Historical1, 99.5 pctl [%]:**	**Rel. difference, 99.5 pctl-mean data, Historical1 [%]:**	**Rel. difference, 99.5 pctl-mean data, RCP8.5 [%]:**
Mean convergence	-14.4	44.4	226.7	368.8
Mean divergence	-13.4	42.2	324.1	462.2

For the change in the divergence profile between events with extreme precipitation and mean events, it is found that the convergence and divergence is stronger during extreme precipitation events for both the historic and future period, which makes it favourable to produce precipitation as more air is lifted and can reach saturation. The results also showed that this difference will be stronger in the future period than it was during the historic. Krishna had an increase of approximate 370 % and 460 % stronger convergence and divergence during the future period, respectively, against 230 % and 320 % higher convergence and divergence during the historic period, respectively. For Godavari, the increase between data on extreme precipitation events and the mean data in the historic period is estimated to be 1050 % and 950 % for convergence and divergence, respectively, while during the future period, the difference will be 1300 and 1200 %, respectively.

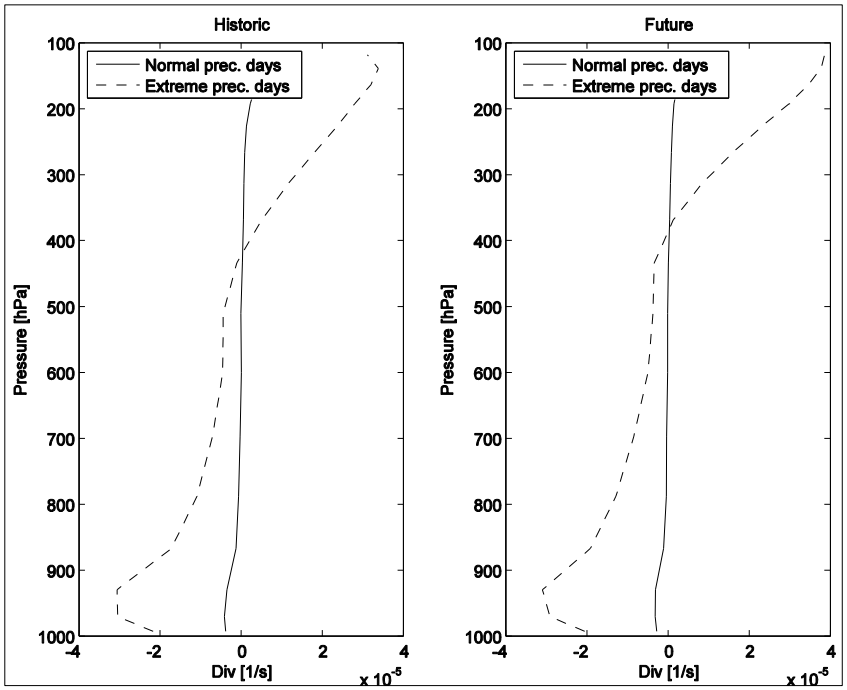

Figure 6.8: The mean horizontal divergence profiles for Godavari over the periods 1960-2000 (left) and 2060-2100 (right) using 6-hourly NorESM data. The Historical1 simulation is used for the historical data, while the RCP8.5 scenario is used for the future data.

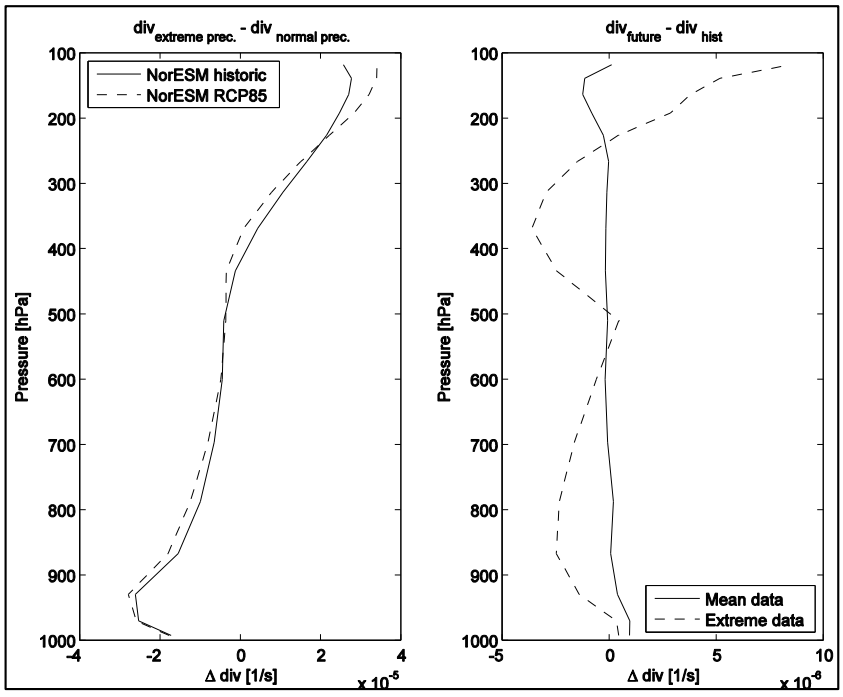

Figure 6.9: Left) The difference between the horizontal divergence at times with extreme precipitation and at times with mean precipitation for both future and historic data. Right) The difference in the horizontal divergence between the future and historic period for both normal and extreme precipitation times. The calculations are performed for 6-hourly data in Godavari during the monsoon months over the periods 1960-2000 and 2060-2000.

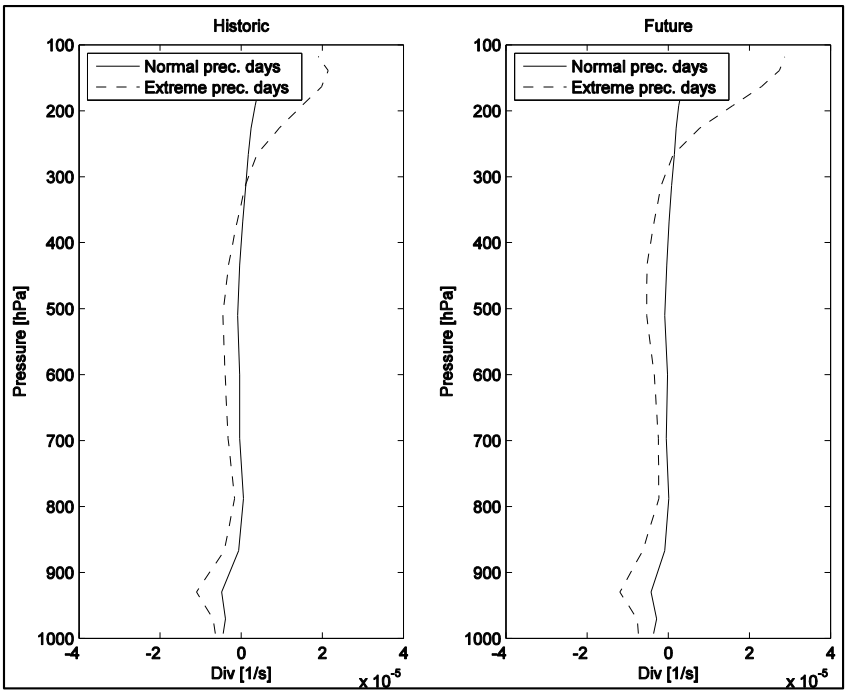

Figure 6.10: The mean horizontal divergence profiles for Krishna over the periods 1960-2000 (left) and 2060-2100 (right) using 6-hourly NorESM data. The Historical1 simulation is used for the historical data, while the RCP8.5 scenario is used for the future data.

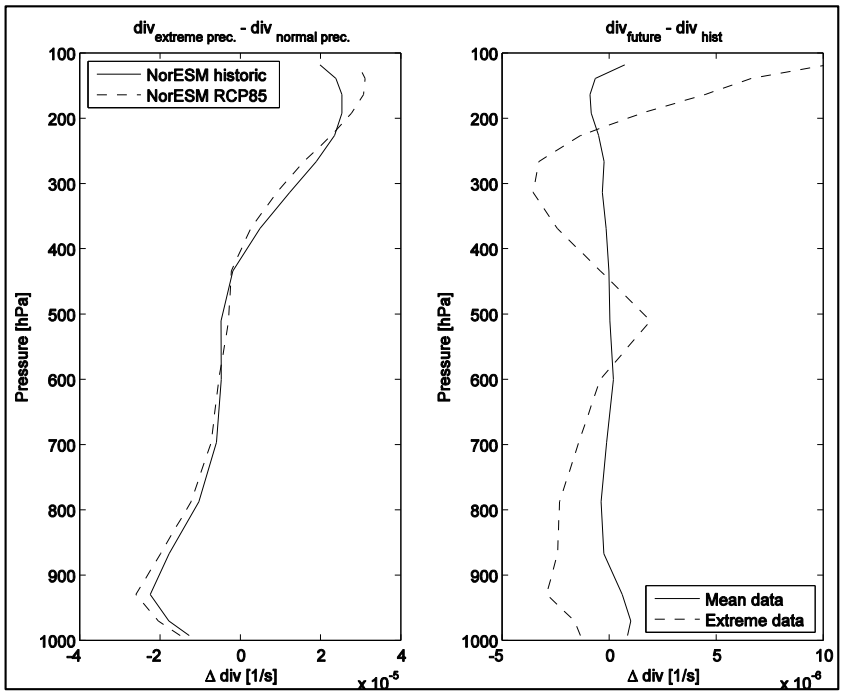

Figure 6.11: Left) The difference between the horizontal divergence at times with extreme precipitation and at times with mean precipitation for both future and historic data. Right) The difference in the horizontal divergence between the future and historic period for both normal and extreme precipitation times. The calculations are performed for 6-hourly data in Krishna during the monsoon months over the periods 1960-2000 and 2060-2000.

During events of extreme precipitation, the wind arrows at the level of maximum convergence (950 hPa) is plotted along with the integrated water vapour transport. As we can see from Figure 6.12 through 6.15, there is a clear convergence pattern over each of the catchments. The moisture is mainly transported from the Bay of Bengal, but a large contribution from the Indian Ocean is also apparent. The values at the origin of the moisture is about 700 kg m^{-1} s^{-1} for the historic data, while it exceeds 900 kg m^{-1} s^{-1} for the RCP8.5 scenario during extreme events. The values over Krishna and Godavari are smaller, with approximately 500 kg m^{-1} s^{-1} during the historical simulation and approximately 700 kg m^{-1} s^{-1} during the RCP8.5 scenario. This implies an increase in moisture transport between the two periods, with a significant relative change of 26% for Godavari and 35% for Krishna (Figure 6.16 and 6.17, and Table 6.5).

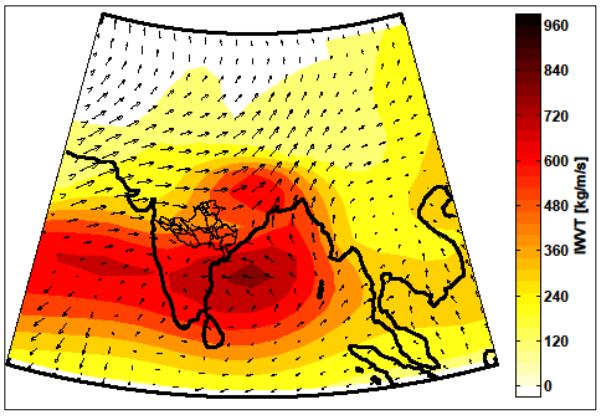

Figure 6.12: The 6-hourly integrated water vapour transport at the events of extreme precipitation over Godavari (black solid line over India) in the period 1960-2000. The NorESM Historical1 simulation during the monsoon months are used in the figure. The arrows indicate the horizontal winds at the level of maximum convergence, i.e. 950 hPa.

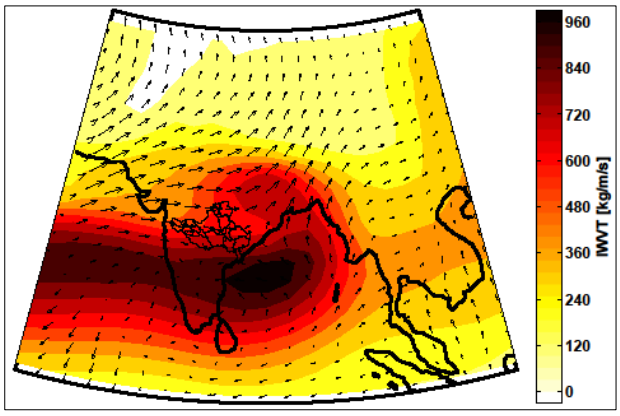

Figure 6.13: The 6-hourly integrated water vapour transport at the events of extreme precipitation over Godavari (black solid line over India) in the period 2060-2100. The NorESM RCP8.5 scenario during the monsoon months has been used in the figure. The arrows indicate the horizontal winds at the level of maximum convergence, i.e. 950 hPa.

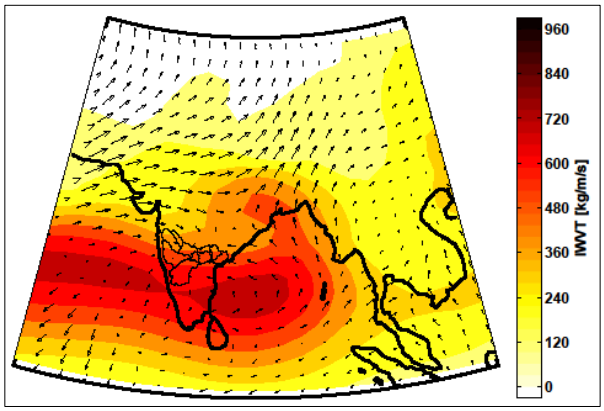

Figure 6.14: The 6-hourly integrated water vapour transport at the events of extreme precipitation over Krishna (black solid line over India) in the period 1960-2000. The NorESM Historical1 simulation during the monsoon months are used in the figure. The arrows indicate the horizontal winds at the level of maximum convergence, i.e. 950 hPa.

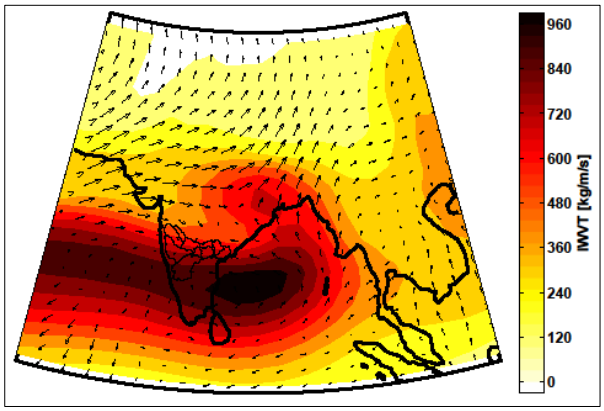

Figure 6.15: The 6-hourly integrated water vapour transport at the events of extreme precipitation over Krishna (black solid line over India) in the period 2060-2100. The NorESM RCP8.5 simulation during the monsoon months are used in the figure. The arrows indicate the horizontal winds at the level of maximum convergence, i.e. 950 hPa.

There is also an increase in the moisture transport at times with extreme precipitation compared to times of mean precipitation (Figure 6.18-6.21). The pattern is very similar for both regions and during both periods, with the largest difference found over the Bay of Bengal and over the Himalayas. Krishna has the lowest difference during the historical period with 52 % stronger extreme events, while in the future the values on extreme precipitation events are 70 % higher than on normal days. For Godavari the difference in moisture transport between extreme and mean events are more even between the historic and future periods, with a relative increase of 74 and 78 %, respectively. All changes in moisture transport between future and historic values, and between values during extreme precipitation events and mean events, are significant.

Table 6.7: The mean values of 6-hourly integrated water vapour transport for mean events and during events with extreme precipitation (99.5 percentile) for both the Historical1 simulation and the RCP8.5 scenario. The relative differences between future and historic values, as well as between extreme and mean data, in which all are significant, are also shown.

Region	Historical1 mean [kg m^{-1} s^{-1}]:	Historical1 99.5 pctl [kg m^{-1} s^{-1}]:	Rel. difference 99.5 pctl data – mean data Historical1 [%]:	RCP8.5 mean [kg m^{-1} s^{-1}]:	RCP8.5 99.5 pctl [kg m^{-1} s^{-1}]:	Rel. difference 99.5 pctl data -mean data RCP8.5 [%]:	Rel. difference Historical1 -RCP8.5, 99.5 pctl data [%]:
Krishna	359.2	542	52	442.4	756.5	69.8	35.1
Godavari	294.2	508.7	73.7	368.6	657	78	25.8

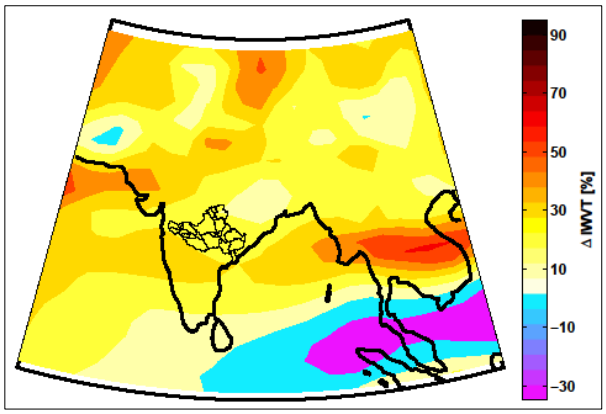

Figure 6.16: Relative change in the 6-hourly integrated water vapour transport between the RCP8.5 (2060-2100) and the Historical1 (1960-2000) data over Godavari (black solid line over India) during extreme precipitation events in the monsoon months. Yellow and red colours indicate an increase, while blue and purple indicate a decrease.

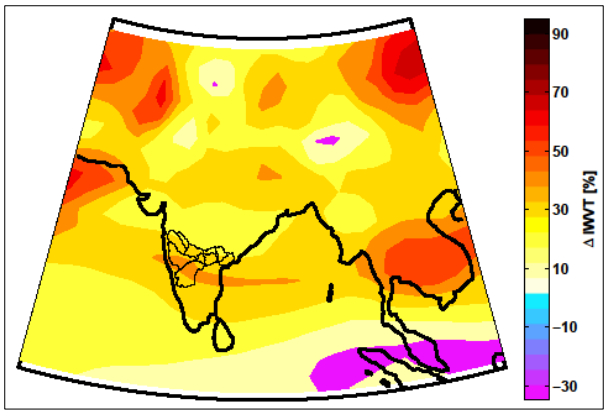

Figure 6.17: Relative change in the 6-hourly integrated water vapour transport between the RCP8.5 (2060-2100) and the Historical1 (1960-2000) data over Krishna (black solid line over India) during extreme precipitation events in the monsoon months. Yellow and red colours indicate an increase, while blue and purple indicate a decrease.

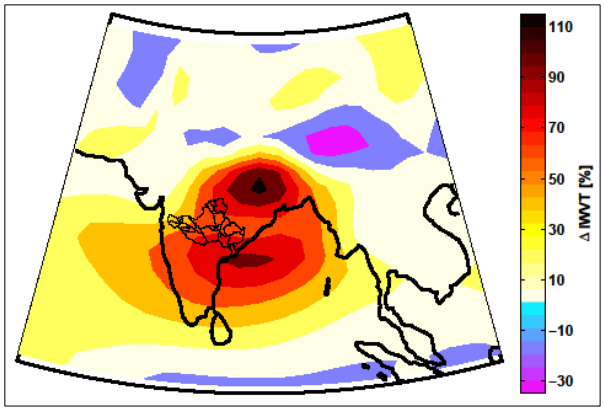

Figure 6.18: Relative difference in 6-hourly integrated water vapour content between events with extreme precipitation and events with normal precipitation for Godavari (black solid line over India) over the period 1960-2000 using the Historical1 simulation.

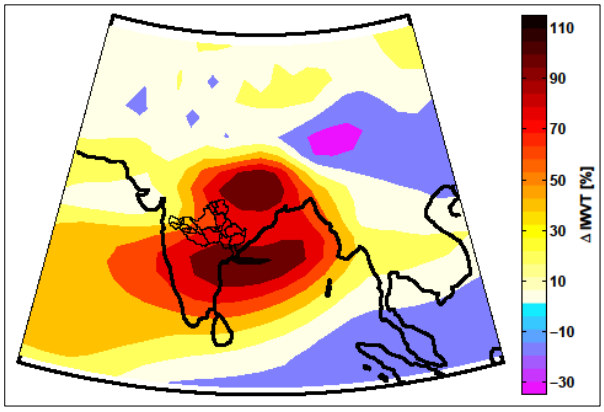

Figure 6.19: Relative difference in 6-hourly integrated water vapour content between events with extreme precipitation and events with normal precipitation for Godavari (black solid line over India) over the period 2060-2100 using the RCP8.5 scenario.

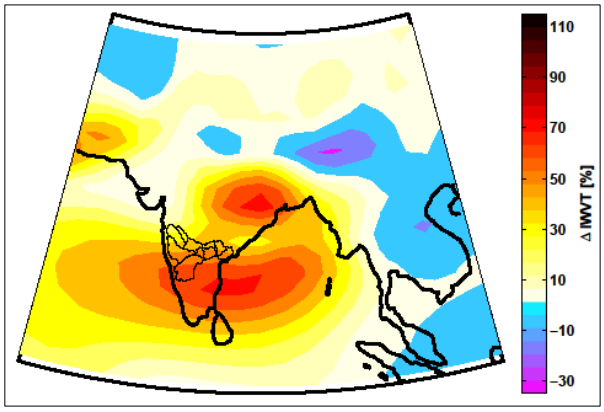

Figure 6.20: Relative difference in 6-hourly integrated water vapour content between events with extreme precipitation and events with normal precipitation for Krishna (black solid line over India) over the period 1960-2000 using the Historical1 simulation.

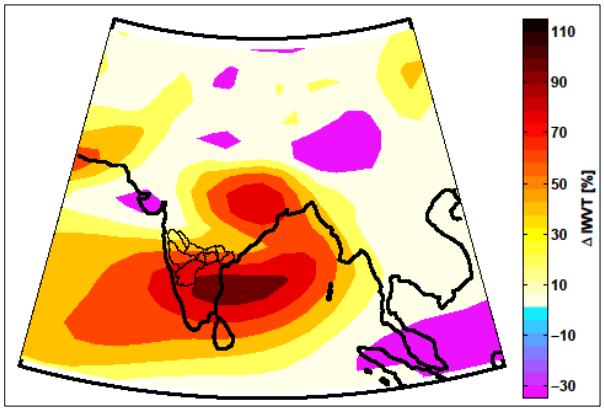

Figure 6.21: Relative difference in 6-hourly integrated water vapour content between events with extreme precipitation and events with normal precipitation for Krishna (black solid line over India) over the period 2060-2100 using the RCP8.5 scenario.

6.3 VERTICAL VELOCITY

The vertical velocity is calculated from Equation 2.12 and 2.13, and the time- and area average is calculated to obtain the vertical profile. Both data during mean events and during 99.5 percentile precipitation events are used in this section, where the data from the Historical1 simulation is used over the period 1960-2000 and the data from the RCP8.5 scenario is used for the period 2060-2100. The significance is calculated using the bootstrap method.

In Figure 6.22 and 6.24 the profiles of the vertical velocity is presented for both mean precipitation and extreme precipitation events, and for both the Historical1 simulation and the RCP8.5 scenario. During mean precipitation events, the vertical velocity has low values close to zero. For the extreme precipitation events, however, the ascent has values up to -0.5 Pa s^{-1} with a maximum at 400 hPa.

The difference between the future and historical vertical velocity, and between the vertical velocity at times with extreme precipitation and at times with mean precipitation, is calculated. The results are presented in Figure 6.23 and 6.25, with negative values indicating an increase (due to the vertical velocity being calculated in pressure-units).

Between Krishna and Godavari, the differences are negligible. Near the top and bottom of the profiles, the differences between future and historic data, as well as between extreme and normal events, are close to zero. For the rest of the profile, the figures show that the vertical velocities during extreme precipitation events will be significantly stronger in the future than they were in the past, while during mean events they will stay the same (Figure 6.23 and 6.25, right picture). The vertical velocity will also be significantly stronger during extreme precipitation events contra mean events, with the largest difference found for the future data (Figure 6.23 and 6.25, left)

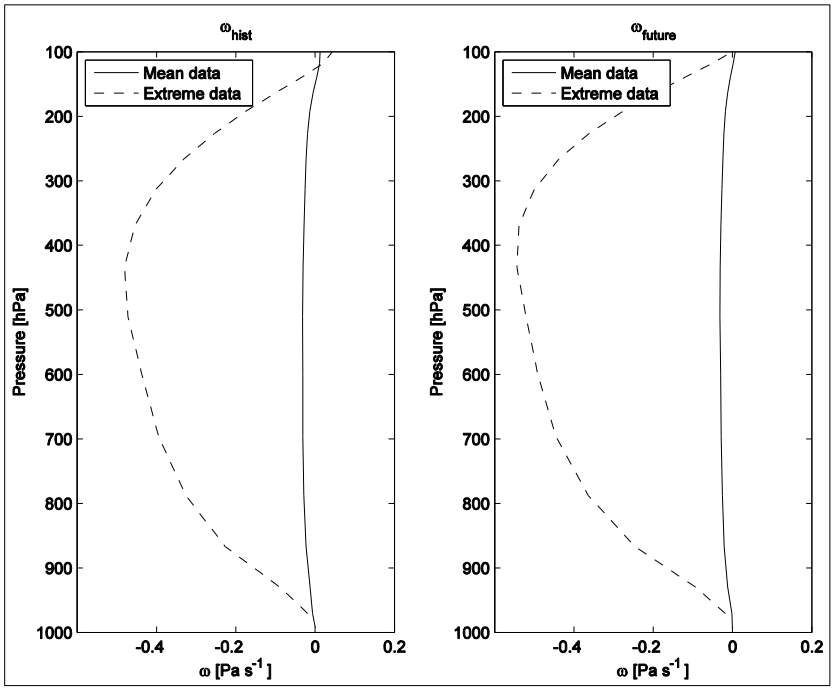

Figure 6.22: The profiles of 6-hourly vertical velocity data (ω) over Godavari for both mean- and extreme precipitation events. The left plot show the profile for the Historical1 simulation over the period 1960-2000 and the right for the RCP8.5 scenario over the period 2060-2100. The mean data over the monsoon months has been applied.

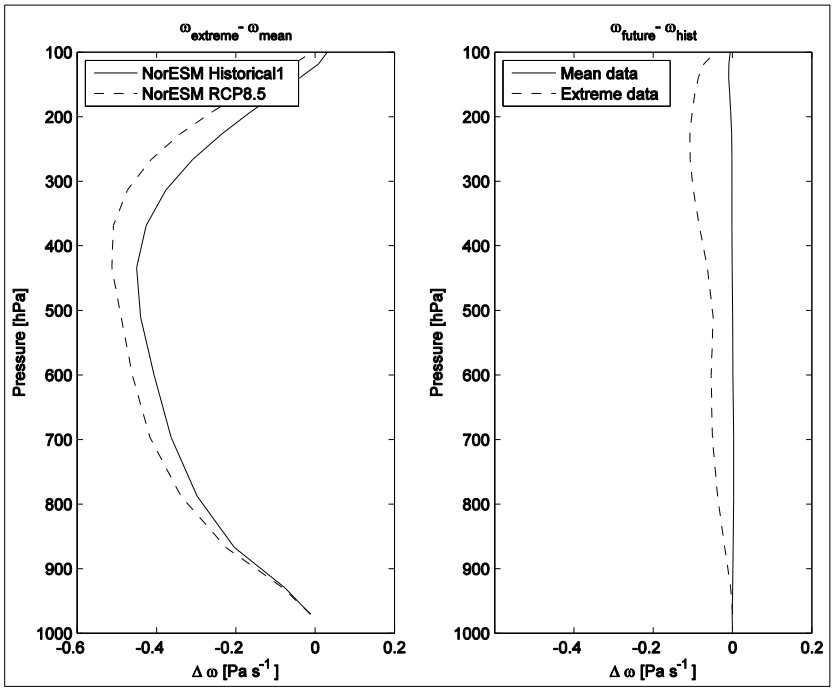

Figure 6.23: Left) The difference between vertical velocity values during mean- and extreme precipitation events, calculated for both future (2060-2100) and historic (1960-2000) data. Right) The difference between future and historic vertical velocity values (ω) during normal- and extreme precipitation events. 6-hourly NorESM Historical1 and RCP8.5 data for Godavari is used over the monsoon months.

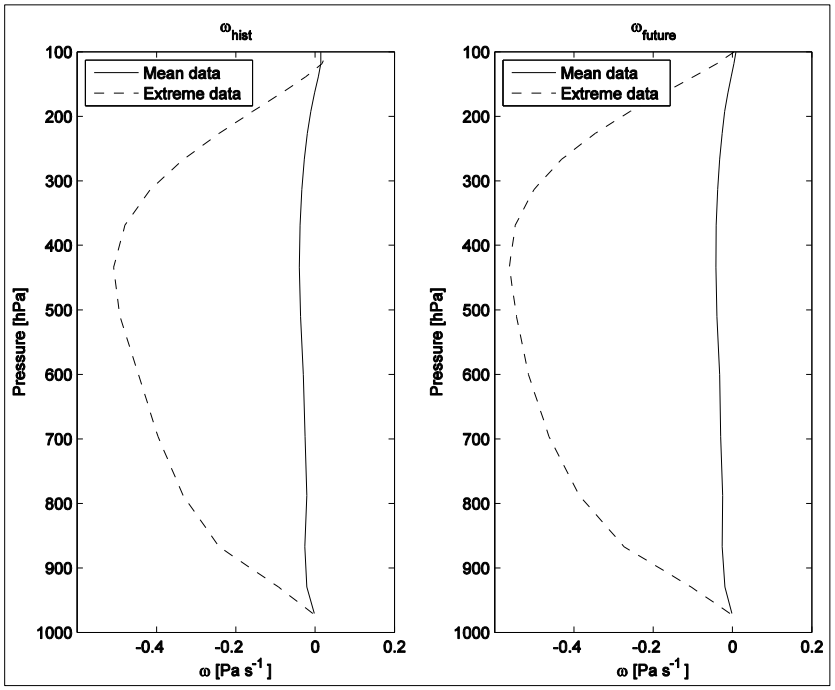

Figure 6.24: The profiles of 6-hourly vertical velocity data (ω) over Krishna for both mean- and extreme precipitation events. The left plot show the profile for the Historical1 simulation over the period 1960-2000 and right for the RCP8.5 scenario over the period 2060-2100. The mean data over the monsoon months has been applied.

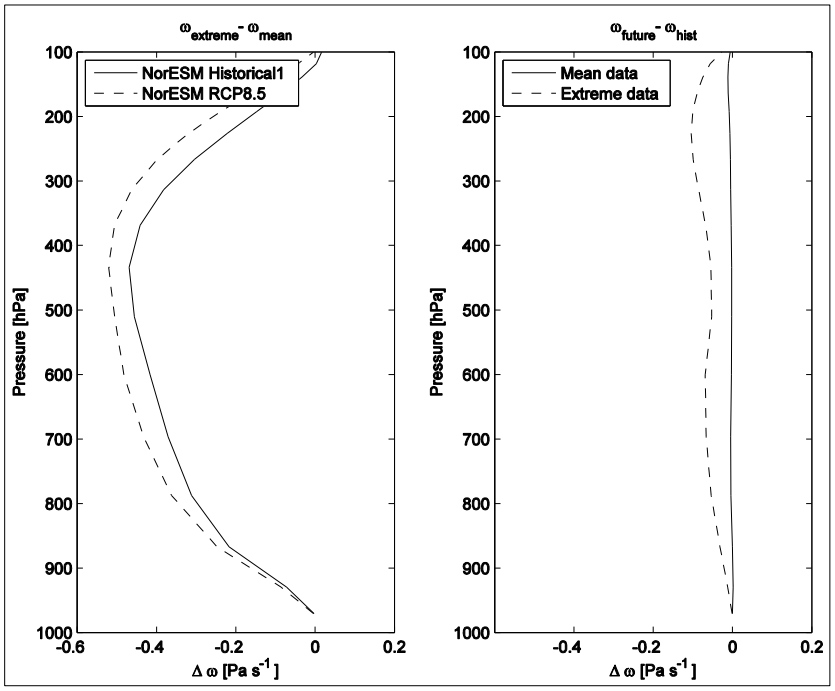

Figure 6.25: Left) The difference between vertical velocity values during mean- and extreme precipitation events, calculated for both future (2060-2100) and historic (1960-2000) data. Right) The difference between future and historic vertical velocity values (ω) during normal- and extreme precipitation events. 6-hourly NorESM Historical1 and RCP8.5 data for Krishna is used over the monsoon months.

6.4 CONVECTIVE AVAILABLE POTENTIAL ENERGY

The convective available potential energy (CAPE) is calculated for both mean- and extreme precipitation events using Equation 2.21 through 2.24. This calculation is performed using the Historical1 simulation over the period 1960-2000 and the RCP8.5 scenario for the period 2060-1000. Taking the area average over the calculations within each catchment, the difference in CAPE between extreme precipitation- and normal events, and between future and historic values, is performed (Table 6.8 and 6.9). The height of LFC and EL is found to be approximately 950 and 400 hPa, respectively, using a Skew-T log-P diagram (Millersville University, 2007).

The amounts of CAPE during extreme precipitation events are found to be ~1860 J/kg for historic data and ~2000 J/kg for future data, which is ~10 % higher than the values on a normal day for Krishna and ~13 % higher for Godavari. The correlation between CAPE and precipitation shows the highest correlation on a normal precipitation day (0.4) compared to on an extreme day (0.1-0.2). The difference in CAPE between future and historic values is significant at a ~7.9 percent increase for both regions and for both normal and extreme days. For the mean data, the correlation is equal to 0.4 for both historic and future data, while for the extreme precipitation events the future data is approximately 0.1 higher (Table 6.10).

Table 6.8: Calculated CAPE for historic (1960-2000) and future (2060-2100) data; during mean- and extreme precipitation events; and the relative difference between them. The calculations are performed with 6-hourly NorESM Historical1 and RCP8.5 data over Godavari.

Data	Historical	Future	Rel. diff [%]
All data [J kg^{-1}]	1651	1782	**7.9**
Extreme events [J kg^{-1}]	1868	2005	**7.4**
Rel. diff [%]	**13.2**	**12.6**	**-**

Table 6.9: Calculated CAPE for historic (1960-2000) and future (2060-2100) data; during mean- and extreme precipitation events; and the relative difference between them. The calculations are performed with 6-hourly NorESM Historical1 and RCP8.5 data over Krishna.

Data	Historical	Future	Rel. diff [%]
All data [J kg^{-1}]	1686	1820	**7.9**
Extreme events [J kg^{-1}]	1857	2005	**7.9**
Rel. diff [%]	**10.2**	**10.2**	**-**

Table 6.10: The correlation between area averaged 6-hourly convective available potential energy (CAPE) during mean and extreme precipitation events within each catchment, as well as for historic (1960-2000) and future (2060-2100) data during the monsoon months.

Region	Historical1	RCP8.5
Mean data		
Godavari	0.4	0.4
Krishna	0.4	0.4
Extreme precipitation events		
Godavari	0.1	0.2
Krishna	0.1	0.2

6.5 TEMPERATURE DISTRIBUTION AND CHANGE

In this section, we investigate the temperature profile at events with mean precipitation and for events with extreme precipitation. The 6-hourly temperature profile averaged over both time and grid points within each catchment is calculated for the Historical1 simulation over the period 1960-2000 and for the RCP8.5 scenario over the period 2060-2100.

The typical temperature profiles for mean data and during events with extreme precipitation events for both historic and future data is presented in Figure 6.26 and 6.27. The profiles are very similar for both regions, with a temperature of approximately 300 K (27 °C) near the ground before it decreases upwards in the atmosphere and becomes negative at approximately 500 hPa.

The results for Krishna show that at 300 hPa the temperature is 2.6 K and 3.9 K higher for historical and future data, respectively, during an extreme event compared to mean precipitation events. The same pattern is seen for Godavari, but the values are slightly higher; 2.2 K for historic and 3.4 K for future data (Figure 6.28 and 6.29).

For the difference between the future and historic values the same pattern is found for each profile; the complete vertical profile becomes warmer in the future, but the upper part of the atmosphere will warm more than the lower part. The maximum heating occurs at 200 hPa, and is 5.6 K for the mean data and 7.5 K during extreme precipitation events. Hence, this uneven distribution is largest for events of extreme precipitation.

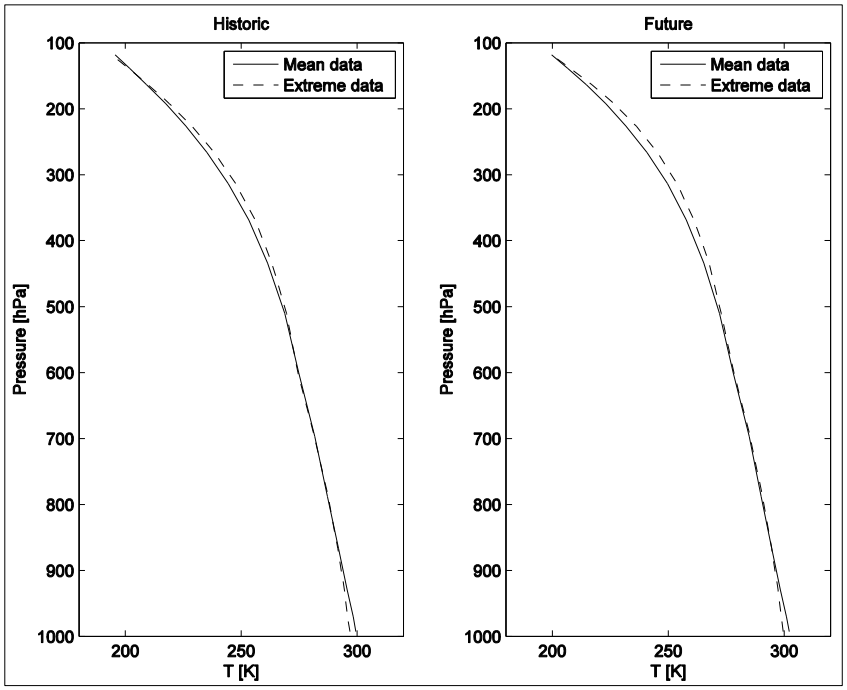

Figure 6.26: The mean 6-hourly temperature profile during the monsoon months for mean data and during events with extreme precipitation for left) the Historical1 simulation (1960-2000), and right) the RCP8.5 scenario (2060-2000) over Godavari.

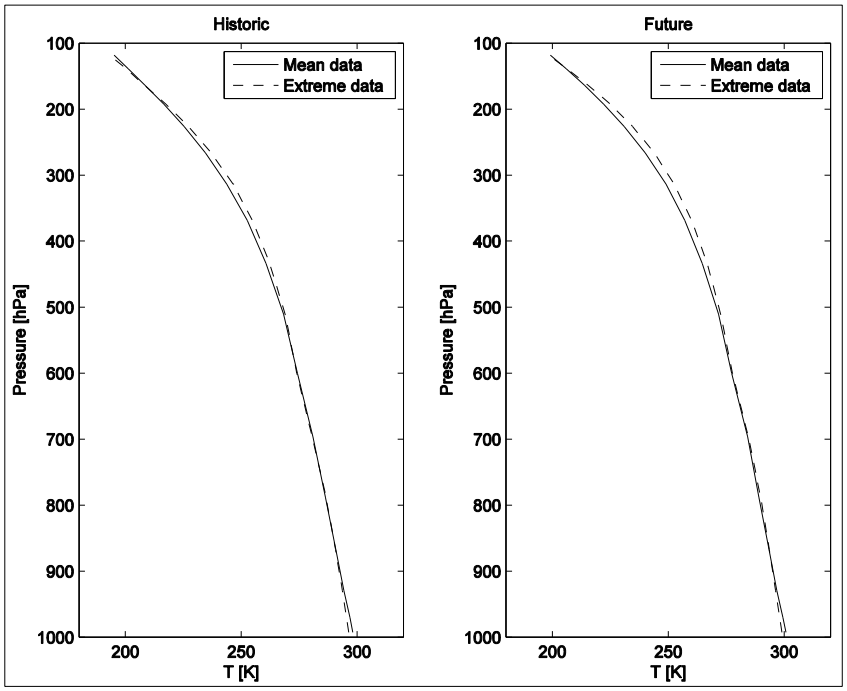

Figure 6.27: The mean 6-hourly temperature profile during the monsoon months for mean data and during events with extreme precipitation for left) the Historical1 simulation (1960-2000), and right) the RCP8.5 scenario (2060-2000) over Krishna.

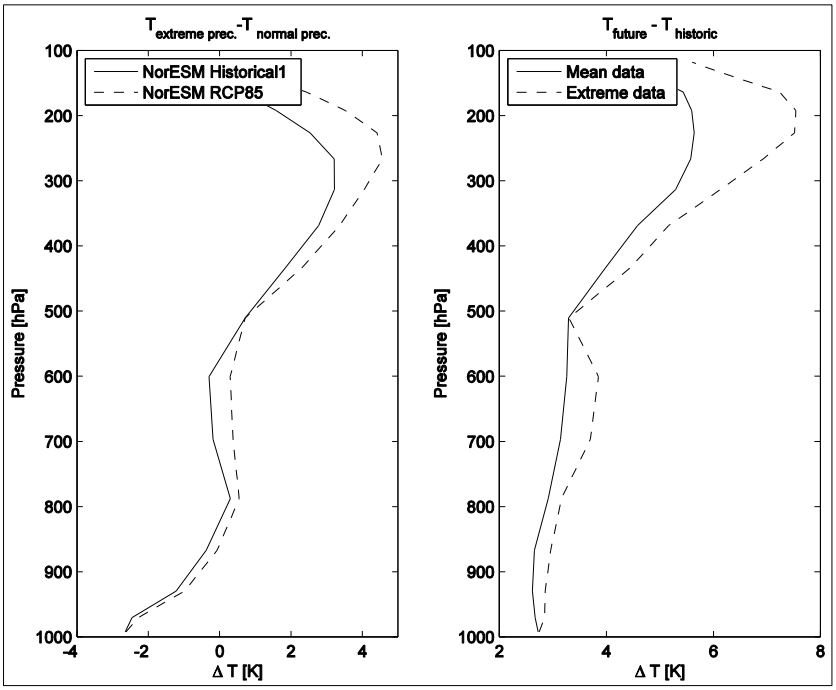

Figure 6.28: Left) Difference in temperature profile between days with extreme precipitation and days with mean precipitation. Right) Difference in temperature profile between the RCP8.5 scenario (2060-2100) and the Historical1 simulation (1960-2000). Both plots are for 6-hourly data during the monsoon months over Godavari.

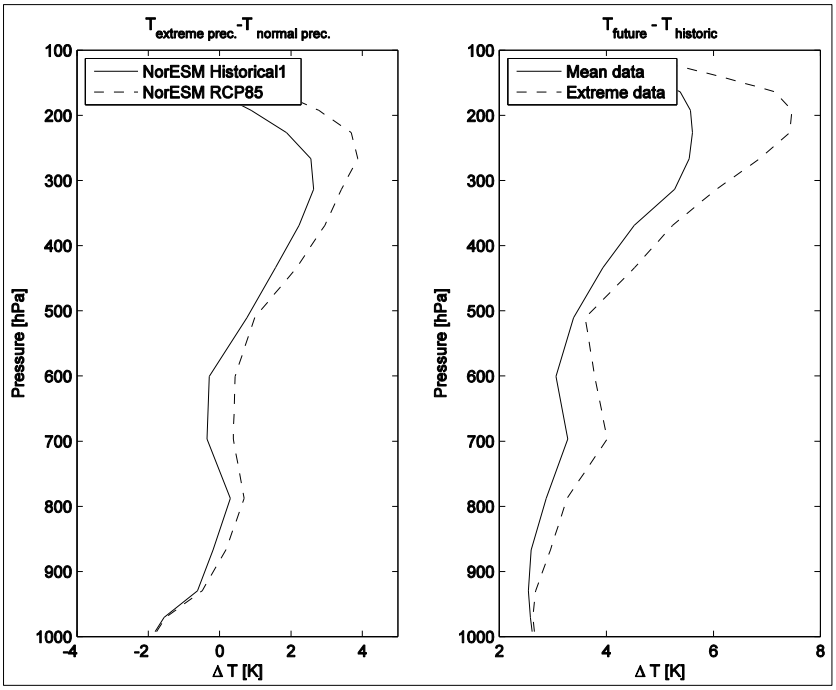

Figure 6.29: Left) Difference in temperature profile between days with extreme precipitation and days with mean precipitation. Right) Difference in temperature profile between the RCP8.5 scenario (2060-2100) and the Historical1 simulation (1960-2000). Both plots are for 6-hourly data during the monsoon months over Krishna.

7. A Simple Precipitation Estimate

With the achieved results in the previous chapter, a simple precipitation estimate is used to investigate how much of the NorESM extreme precipitation that can be understood in terms of simple moist adiabatic ascent. The NorESM 6-hourly temperature data is used to calculate the saturation vapour pressure through the Clausius-Clapeyron relation, which, along with the pressure levels, is further used to calculate the specific humidity at saturation. To obtain the condensation rate, the change in specific humidity with pressure level is multiplied with the vertical velocity:

$$\frac{dq_s}{dt} = \omega \cdot \frac{dq_s}{dp} = \omega \cdot \frac{q_s T}{p} \cdot \frac{L_v R_d - c_p R_v T}{c_p R_v T^2 + q_s L_v^2} \tag{7.1}$$

where ω is the vertical velocity, q_s is the specific humidity, T is temperature, L_v is the latent heat of vaporization, $R_d \; and \; R_v$ are the gas constants for dry and moist air, respectively, and c_p is the specific heat capacity at constant pressure. To calculate the condensation, the times where $\frac{dq_s}{dt} < 0$ are selected (i.e. upward velocities and $\frac{dq_s}{dp} > 0$), as the content of specific humidity decreases as it transforms into liquid water.

Finally, to obtain the precipitation rate from moist adiabatic ascent under the assumption that all condensed water fall out immediately, the mass weighted integrated condensation rate is calculated:

$$Pr = -\frac{1}{g} \int_{p_0}^{p} \frac{dq_s}{dt} dp \tag{7.2}$$

The extreme precipitation amounts and the number of extreme events are calculated the same way as for the NorESM simulations, i.e. defined as the 6-hourly events exceeding the 99.5 percentile of the historic and future values, while for the number of extreme events in the future they are calculated relative to the historic percentile.

A comparison between the NorESM historic mean and extreme precipitation and the moist adiabatic estimate is presented in Figure 7.1 and 7.3, and in addition the correlation between the two are given. The results show that the extreme precipitation from the moist adiabatic estimate is underestimated by approximately 20 mm compared to values from the much more complicated NorESM-model, both for the historic and future data. Using only the dates with

an extreme event from NorESM, a correlation of 0.4 for Krishna and 0.5 for Godavari is found, while looking at all events the correlation increased to 0.8 in both regions. For the future scenario, the correlations are similar (Figure 7.2 and 7.4). The correlations may be higher when including all precipitation data because the deviations between NorESM and the simple precipitation model are largest for extreme events.

The difference between future and historic extreme precipitation intensity is slightly smaller compared to NorESM-values, while for the number of extreme events the trends from the simple precipitation estimate is highly overestimated. For Godavari, the relative change in intensity has an increase of 25 % using the moist adiabatic model, while it is 30 % for NorESM, and for Krishna the results show 29 % against 34 %, respectively. The trends in the number of extreme events show twice the increase for Krishna (95 % against 175 %) and three times the increase for Godavari (41 % against 120 %) in the simple estimate compared to NorESM. To sum up, the simple precipitation estimate predicts about the same increase in extreme precipitation amount, but a higher number of events.

A possible solution for the underestimated precipitation in the simple moist adiabatic estimate is due to the exclusion of diabatic processes such as radiative cooling of the air. In the NorESM simulation, air is mixed into the ascending air parcel from the surroundings, and if this air is cooler than the parcel the condensation rate increases. In the simple precipitation model the air follows the moist adiabatic lapse rate and is isolated from its surroundings. This air will thus be warmer than in the NorESM simulation and will have a lower condensation rate, resulting in less precipitation. The assumption that the air in the simple model always is saturated may be an explanation for the high number of extreme events in the future, as the moisture is estimated to increase in accordance with the global warming.

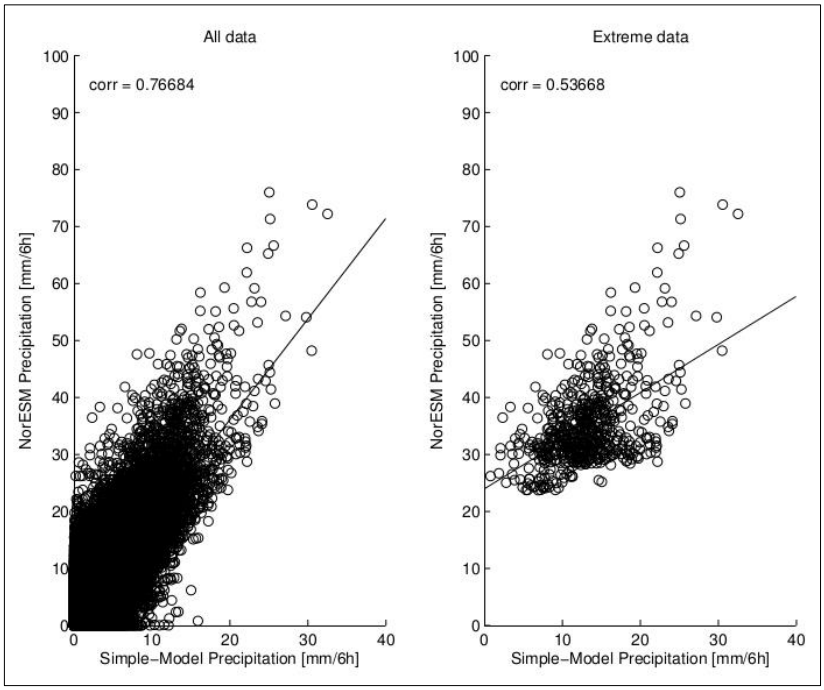

Figure 7.1: Comparison of 6-hourly NorESM Historical1 simulated precipitation to 6-hourly moist adiabatic generated precipitation calculated with variables from Historical1 in Godavari.

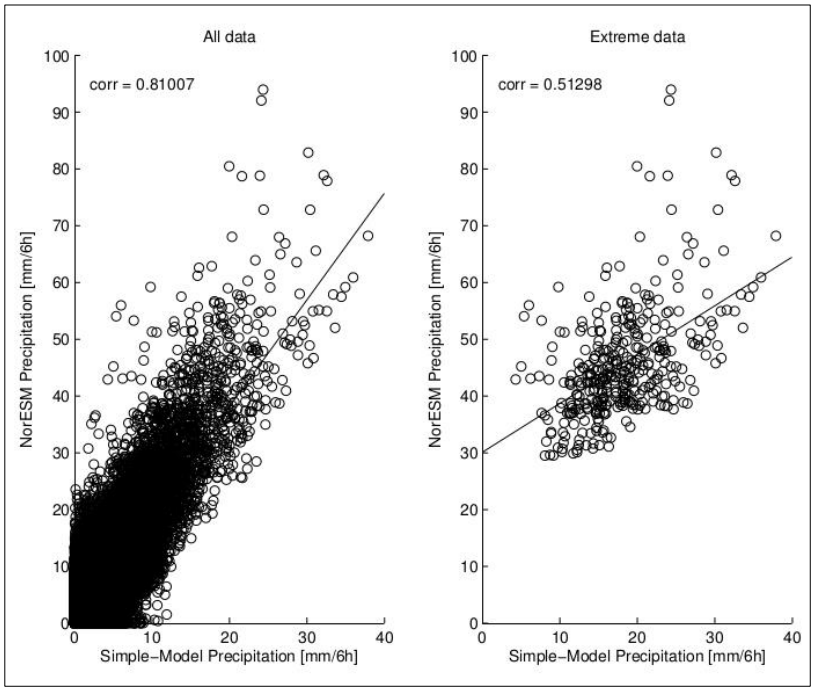

Figure 7.2: Comparison of 6-hourly NorESM RCP8.5 scenario precipitation to 6-hourly moist adiabatic generated precipitation calculated with variables from RCP8.5 in Godavari.

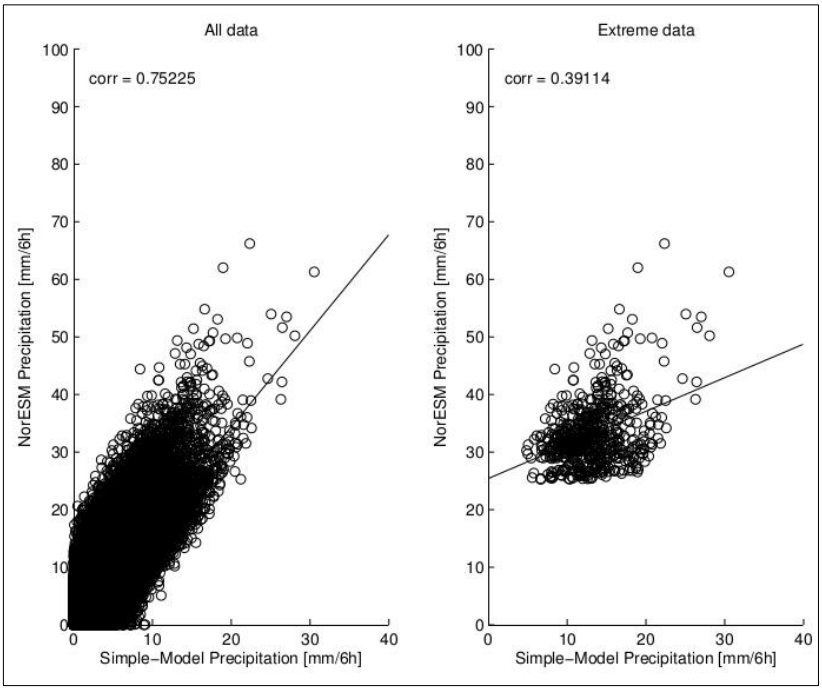

Figure 7.3: Comparison of 6-hourly NorESM Historical1 simulated precipitation to 6-hourly moist adiabatic generated precipitation calculated with variables from Historical1 in Krishna.

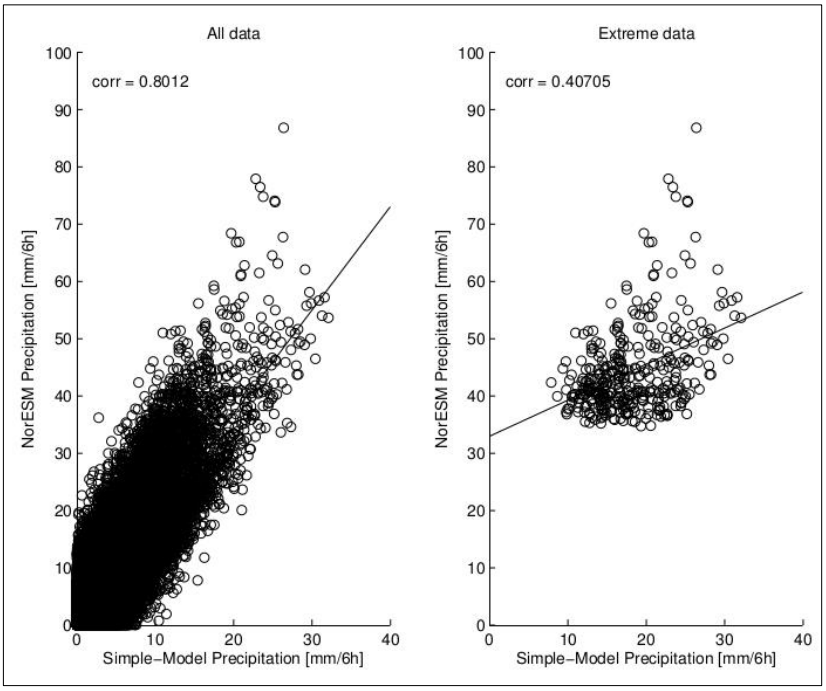

Figure 7.4: Comparison of 6-hourly NorESM RCP8.5 scenario precipitation to 6-hourly moist adiabatic generated precipitation calculated with variables from RCP8.5 in Krishna.

8. Discussion

In Section 6.2, the results shows that the divergence is stronger than the convergence during the monsoon. Physically this means that more air is removed aloft than is supplied at the ground, resulting in a lower pressure over the mean vertical profile. In conjunction with the large monsoon circulation, this lower pressure results in a stronger meridional pressure gradient, which will enhance the circulation.

For the detected mean vertical divergence profile, there is clearly a connection to the extreme precipitation. Studying the difference between values during mean and extreme precipitation events, the convergence at 950 hPa and the divergence at 150 hPa is stronger during extremes, indicating more ascending air. In conjunction with the estimated increase in the future extreme precipitation amounts there are also estimated an increase in the divergence profile. These results coincides well with the results obtained in the vertical velocity calculations as it is found that the upward velocity is larger during extreme events and the values during extreme events will be stronger in the future.

The integrated water vapour transport into the area of convection is of course also crucial for the precipitation to occur, and as observed in Figure 6.12-6.15 the integrated water vapour comes from the Bay of Bengal and the large scale monsoon flow into the two regions. In the future, this transport will increase by approximately 25-30% over Godavari and 30-40 % over Krishna, which facilitates more precipitation if it condenses out. In addition, the figures presenting the difference in moisture transport between extreme and mean precipitation events (Figure 6.18-6.21) indicate that the transport is approximately twice that of the mean amounts during extreme-events. The increased circulation along with the increased temperatures may explain why the integrated water vapour transport increases. First of all, due to the Clausius-Clapeyron relation (Section 2.1) the air can contain more moisture with increasing temperatures, thus being able to increase the water vapour flux from ocean to air through evaporation. Secondly, as the circulation increases, stronger winds will blow over the ocean and increase the stress against the sea surface. This results in spray (mixing of water droplets into the air) which in turn evaporates, increasing the humidity and decreasing the temperature of the air (Smith, 1989).

The temperature profile is on the other hand working against convection. During extreme events, the temperature near the ground becomes cooler while the upper levels become warmer, resulting in a more stable, and less convective, column of air. The cooling in the

lower layers may be due to the evaporation from the ground during precipitation, while the heating above may result from condensation. Some of this heating and cooling through the atmosphere might also be explained by cloud radiative heating (CRH). Johansson et al. (2015) studied the effect on CRH by different types of clouds during the monsoon months over India. The result showed that alto- and nimbostratus clouds along with deep convection warms the middle troposphere, while cooling the upper troposphere. At the base of the tropical tropopause layer (TTL) (transition layer between troposphere and stratosphere (Fueglistaler et al., 2009)) the cirrus clouds heats up the air and also plays an important role in the transport of air from the troposphere to the stratosphere. At the surface, stratiform clouds and deep convection cause significantly cooling, due to the net cloud radiative effect (CRE) being negative.

The same pattern is observed between historic and future data. The divergence and convergence tends to become stronger during extreme events in the future (especially for Krishna, but also weakly for Godavari), as well as an enhancement in the vertical velocity, which both are favourable for enhanced precipitation. In the temperature profile, however, it is observed an increase in stabilization between the future and the historic values, but compared to the difference between extreme and normal precipitation events, now the change is positive over the whole column, which is a direct result of the global warming. The higher temperature increase aloft may be a result from increased atmospheric moisture aloft and possible higher cloud amounts due to the effects from the CRH explained in the previous paragraph.

From the equations in Section 2.4, CAPE depends on both moisture content and on the temperature profile. DeMott and Randall (2004) found that the trends in CAPE are primarily driven by same-signed changes in low-level moisture, while the temperature profile plays a secondary role and has a more random impact on the precipitation. This implies that the more stable temperature profile estimated in the future has less impact on the creation of CAPE than the estimated increase in moisture, which is observed as the CAPE will increase in the future too. The calculated values of CAPE during extreme precipitation events over the period 2060-2100 barely exceeds 2000 J kg^{-1}, which is an increase of 8 % compared to historic values and 10-13 % higher than on mean precipitation events. These values are low compared to the expected values of strong and extreme convection, which are typically around 4000 J kg^{-1} (Wallace and Hobbs, 2006). However, because of continuous convection over long

periods during the monsoon, the CAPE may not be able to obtain very large amounts as the convective activity removes it before it manage to reach the large values.

Summing up, the results show that the divergence, the vertical velocity and the moisture transport are working as drivers for the extreme precipitation, while the temperature is working against it. Because extreme precipitation events does happen, this implies that the temperature has a smaller influence than the other variables. The same result was found in a research by Sørland (2015) where the correlation between temperature and extreme precipitation was found to equal -0.17 at 950 hPa and 0.03 at 750 hPa.

8.1 THE IMPACT OF VERTICAL VELOCITY AND MOISTURE ON THE PRECIPITATION AMOUNTS

To investigate which of the remaining variables, i.e. vertical velocity and water vapour, the extreme precipitation is most dependent on, a multiple linear regression procedure is performed. Based on Equation 3.1 and 3.3, the relationship between 6-hourly extreme precipitation (99.5 percentile, taken from the gridpoints inside each catchment), vertical velocity and specific humidity has been calculated:

$$Pr_{regress} = \frac{\partial Pr}{\partial \omega_{\max corr}} \cdot \omega_{\max corr} + \frac{\partial Pr}{\partial q_{int}} \cdot q_{int} + b_0 \tag{6.1}$$

where $\omega_{\max corr}$ indicate that we use the vertical velocity at the level of maximum correlation with the precipitation (700 hPa for the Historical1 simulation, and 600 hPa for the RCP8.5 scenario), and q_{int} indicate that we use the column integrated specific humidity. $Pr_{regress}$ is the precipitation calculated using regression analysis, Pr is the precipitation obtained from NorESM-data, and b_0 is the y-intercept value. To get coinciding data between the independent variables and the extreme precipitation, the extreme precipitation data has been accumulated for non-overlapping periods.

8.1.1 NorESM Historical simulation

The results from the multiple linear regression can be seen in Table 8.1 through 8.4. The highest correlation between Pr and $Pr_{regress}$ is found over Godavari, with a value of 0.66. In addition, the correlation between the specific humidity and the vertical velocity is almost non-existent (-0.09), and we can thus assume independence between the variables. Both the

correlation between Pr and each of the independent variables, as well as the standardized regression coefficients, show that the extreme precipitation intensity variability depends mostly on the vertical velocity variability. This variable has both the highest absolute correlation (0.58) and the standardized regression coefficients indicates that a 1 standard deviation in the vertical velocity gives a 0.55 STD change in precipitation.

Table 8.1: The correlation between the 6-hourly 99.5 percentile Historical1 precipitation and the regression-calculated precipitation, the specific humidity and the vertical velocity at the coinciding times, respectively. The data in brackets are the confidence intervals for the 5% significance level calculated using the bootstrap method. The data is for Godavari over the period 1960-2000.

Variable:	**Pr**	**q**	**ω**
Pr	1		
$Pr_{regress}$	0.66 [0.59,0.72]		
q	0.36 [0.28,0.45]	1	
ω	-0.58 [-0.64,-0.52]	-0.09 [-0.19, 0]	1

Table 8.2: The correlation between the 6-hourly 99.5 percentile Historical1 precipitation and the regression-calculated precipitation, the specific humidity and the vertical velocity at the coinciding times, respectively. The data in brackets are the confidence intervals for the 5% significance level calculated using the bootstrap method. The data is for Krishna over the period 1960-2000.

Variable:	**Pr**	**q**	**ω**
Pr	1		
$Pr_{regress}$	0.47 [0.39,0.54]		
q	0.33 [0.26,0.41]	1	
ω	-0.44 [-0.51,-0.36]	-0.41 [-0.48, -0.34]	1

For Krishna, the same relationship among the variables is found, but the values are lower than they are for Godavari. The correlation between Pr and $Pr_{regress}$ has a value of 0.47, but due to a correlation of -0.41 between the vertical velocity and the specific humidity they show dependence and therefore it is not possible to properly identify which of the variables that influences the precipitation the most.

Table 8.3: Multiple linear regression values for the 6-hourly Historical1 simulation over Godavari. The values used as input are 6-hourly gridpoint data over the period 1960-2000. q_{int} is the integrated specific humidity over the atmospheric column while $\omega_{max\ corr}$ is the vertical velocity at the level of maximum correlation with the precipitation. b-weight is the change in precipitation per variable-unit, while β-weight is the standardized, unit-less change. b_{min} and b_{max} (β_{min} and β_{max}) CI defines the confidence interval for the 5% significance level, respectively, calculated using the F-test. Together with the p-value, the CI tells if the weightings are significant. $\frac{dPr}{dq_{int}}$ and $\frac{dPr}{d\omega_{max\ corr}}$ are the change in extreme precipitation with a change in specific humidity and vertical velocity, respectively, while b_0 is the intercept value.

Variable	**b-weight**	**b_{min} CI**	**b_{max} CI**	
$\frac{dPr}{dq_{int}}\left[\frac{mm}{\frac{kg}{kg}}\right]$	6.32E+04	5.09E+04	7.55E+04	
$\frac{dPr}{d\omega_{max\ corr}}\left[\frac{mm}{\frac{Pa}{s}}\right]$	-27.6	-30.6	-24.6	
b_0	-15.2	-22.9	-7.5	
	β-weight [SD/SD]	**β_{min} CI [SD/SD]**	**β_{max} CI [SD/SD]**	**p-value**
$\frac{dPr}{dq_{int}}$	0.3	0.3	0.4	<0.001
$\frac{dPr}{d\omega_{max\ corr}}$	-0.6	-0.6	-0.5	<0.001
b_0	0	-0.1	0.1	<0.001

Table 8.4: Multiple linear regression values for the 6-hourly Historical1 simulation over Krishna. The values used as input are 6-hourly gridpoint data over the period 1960-2000. q_{int} is the integrated specific humidity over the atmospheric column while $\omega_{max\ corr}$ is the vertical velocity at the level of maximum correlation with the precipitation. b-weight is the change in precipitation per variable-unit, while β-weight is the standardized, unit-less change. b_{min} and b_{max} (β_{min} and β_{max}) CI defines the confidence interval for the 5% significance level, respectively, calculated using the F-test. Together with the p-value, the CI tells if the weightings are significant. $\frac{dPr}{dq_{int}}$ and $\frac{dPr}{d\omega_{max\ corr}}$ are the change in extreme precipitation with a change in specific humidity and vertical velocity, respectively, while b_0 is the intercept value.

Variable	b-weight	b_{min} CI	b_{max} CI	
$\frac{dPr}{dq_{int}}\left[\frac{mm}{\frac{kg}{kg}}\right]$	3.01E+04	1.72E+04	4.29E+04	
$\frac{dPr}{d\omega_{max\ corr}}\left[\frac{mm}{\frac{Pa}{s}}\right]$	-14.7	-17.9	-11.6	
b_0	9.5	2.3	16.7	
	β-weight [SD/SD]	**β_{min} CI [SD/SD]**	**β_{max} CI [SD/SD]**	**p-value**
$\frac{dPr}{dq_{int}}$	0.2	0.1	0.3	<0.001
$\frac{dPr}{d\omega_{max\ corr}}$	-0.4	-0.4	-0.3	<0.001
b_0	0	-0.1	0.1	0.0096

In contrast to the lower correlation between the modelled and the regressed extreme precipitation, Krishna is more affected by a change in specific humidity and vertical velocity than Godavari is. This may be due to the correlation between the specific humidity and the vertical velocity in Krishna, which is absent over Godavari. Because the correlation is negative it means that with increasing vertical velocity (a more negative value) an increase in the specific humidity is expected, which both are favourable for enhanced precipitation. For Godavari we find that an increase in the vertical velocity with 1 ms^{-1} leads to an increase in extreme precipitation of 28 mm/6h, while for Krishna it is 15 mm/6h. Looking at the specific humidity, a typical change in the order of 1×10^{-4} leads to an increase of 6 mm/6h over Godavari, while for Krishna the same increase will give approximately 3 mm/6h higher extreme precipitation. Even though Godavari seems to be the region that is most affected, including the intercept value, Krishna is overall the region with the highest change in precipitation in conjunction with a one-unit change in vertical velocity and specific humidity, giving a value of 28 mm/6h, contra Godavari with 19 mm/6h.

8.1.2 RCP8.5

For the future extremes, Godavari still has the highest correlation (0.64) between the modelled and the regressed extreme precipitation. The dependence between the specific humidity and the vertical velocity in Krishna has increased to a correlation of -0.19 (Table 8.6), while for Godavari they can be assumed non-correlated with a value of
-0.06 (Table 8.5). Again, the vertical velocity is the most influencing variable as seen both in the standardized regression coefficients and in the correlation with the extreme precipitation.

Table 8.5: The correlation between the 6-hourly 99.5 percentile RCP8.5 precipitation and the regression-calculated precipitation, the specific humidity and the vertical velocity at the coinciding times, respectively. The data in brackets are the confidence intervals for the 5% significance level calculated using the bootstrap method. The data is for Godavari over the period 2060-2100.

Variable	Pr	q	ω
Pr	1		
$Pr_{regress}$	0.64 [0.58,0.69]		
q	0.40 [0.31,0.47]	1	
ω	-0.52 [-0.60,-0.44]	-0.06 [-0.18,0.06]	1

Table 8.6: The correlation between the 6-hourly 99.5 percentile RCP8.5 precipitation and the regression-calculated precipitation, the specific humidity and the vertical velocity at the coinciding times, respectively. The data in brackets are the confidence intervals for the 5% significance level calculated using the bootstrap method. The data is for Krishna over the period 2060-2100.

Variable	**Pr**	**q**	**ω**
Pr	1		
$Pr_{regress}$	0.49 [0.42,0.56]		
q	0.26 [0.19,0.33]	1	
ω	-0.46 [-0.53,-0.38]	-0.19 [-0.29,-0.09]	1

In accordance with the historical values, Krishna shows the largest change in precipitation with a one-unit change in specific humidity and vertical velocity compared to Godavari (34 mm/6hr against 10 mm/6hr, respectively). At a first glance, it might seem that the sensitivity of extreme precipitation intensity to specific humidity and vertical velocity has decreased over Godavari and increased over Krishna for future data compared to historic (Table 8.3 and 8.4 compared to Table 8.7 and 8.8, respectively). However, the results of the historic and future regression analysis are not significantly different, and we thus assume there is no change between them.

Table 8.7: Multiple linear regression values for the 6-hourly RCP8.5 scenario over Godavari. The values used as input are 6-hourly gridpoint data over the period 2060-2100. q_{int} is the integrated specific humidity over the atmospheric column while $\omega_{max\ corr}$ is the vertical velocity at the level of maximum correlation with the precipitation. b-weight is the change in precipitation per variable-unit, while β-weight is the standardized, unit-less change. b_{min} and b_{max} (β_{min} and β_{max}) CI defines the confidence interval for the 5% significance level, respectively, calculated using the F-test. Together with the p-value, the CI tells if the weightings are significant. $\frac{dPr}{dq_{int}}$ and $\frac{dPr}{d\omega_{max\ corr}}$ are the change in extreme precipitation with a change in specific humidity and vertical velocity, respectively, while b_0 is the intercept value.

Variable	b-weight	b_{min} CI	b_{max} CI	
$\frac{dPr}{dq_{int}}\left[\frac{mm}{\frac{kg}{kg}}\right]$	7.22E+04	5.66E+04	8.79E+04	
$\frac{dPr}{d\omega_{max\ corr}}\left[\frac{mm}{\frac{Pa}{s}}\right]$	-28.9	-33.5	-24.4	
b_0	-25.9	-38.4	-13.4	
	β-weight [SD/SD]	**β_{min} CI [SD/SD]**	**β_{max} CI [SD/SD]**	**p-value**
$\frac{dPr}{dq_{int}}$	0.37	0.3	0.4	<0.001
$\frac{dPr}{d\omega_{max\ corr}}$	-0.50	-0.6	-0.4	<0.001
b_0	0	-0.1	0.1	<0.001

Table 8.8: Multiple linear regression values for the 6-hourly RCP8.5 scenario over Krishna. The values used as input are 6-hourly gridpoint data over the period 2060-2100. q_{int} is the integrated specific humidity over the atmospheric column while $\omega_{max\ corr}$ is the vertical velocity at the level of maximum correlation with the precipitation. b-weight is the change in precipitation per variable-unit, while β-weight is the standardized, unit-less change. b_{min} and b_{max} (β_{min} and β_{max}) CI defines the confidence interval for the 5% significance level, respectively, calculated using the F-test. Together with the p-value, the CI tells if the weightings are significant. $\frac{dPr}{dq_{int}}$ and $\frac{dPr}{d\omega_{max\ corr}}$ are the change in extreme precipitation with a change in specific humidity and vertical velocity, respectively, while b_0 is the intercept value.

Variable	**b-weight**	**b_{min} CI**	**b_{max} CI**	
$\frac{dPr}{dq_{int}}\left[\frac{mm}{\frac{kg}{kg}}\right]$	3.15E+04	1.54E+04	4.77E+04	
$\frac{dPr}{d\omega_{max\ corr}}\left[\frac{mm}{\frac{Pa}{s}}\right]$	-20.2	-24.5	-15.9	
b_0	10.1	-1.8	22.1	
	β-weight [SD/SD]	**β_{min} CI [SD/SD]**	**β_{max} CI [SD/SD]**	**p-value**
$\frac{dPr}{dq_{int}}$	0.2	0.1	0.3	<0.001
$\frac{dPr}{d\omega_{max\ corr}}$	-0.4	-0.5	-0.3	<0.001
b_0	0	-0.1	0.1	0.098

The scatterplots in Figure 8.1 through 8.4 presents the same results as in Chapter 6, i.e. a higher content of specific humidity (moisture) will give an increased amount of precipitation, and similar for an increase in upward vertical velocity. The scatterplots also show that the precipitation obtained using regression analysis has lower values than the precipitation simulated by the NorESM (maximum regressed precipitation is approximately 50 mm/6h while the maximum precipitation in NorESM is approximate 70 mm/6hr for the Historical1 simulation, and respectively 60 and 90 mm/6hr for the RCP8.5 scenario). An explanation to this may be related to the exclusion of stability in the regression estimate. As mentioned in Section 2.4, it is necessary to have an amount of CIN such that the air can build up enough energy (CAPE) to obtain heavy amounts of precipitation. As we found in Section 6.4 the amounts of CAPE are a bit higher during extreme events, and the exclusion of this term may be enough not to achieve large enough amounts for the extreme cases.

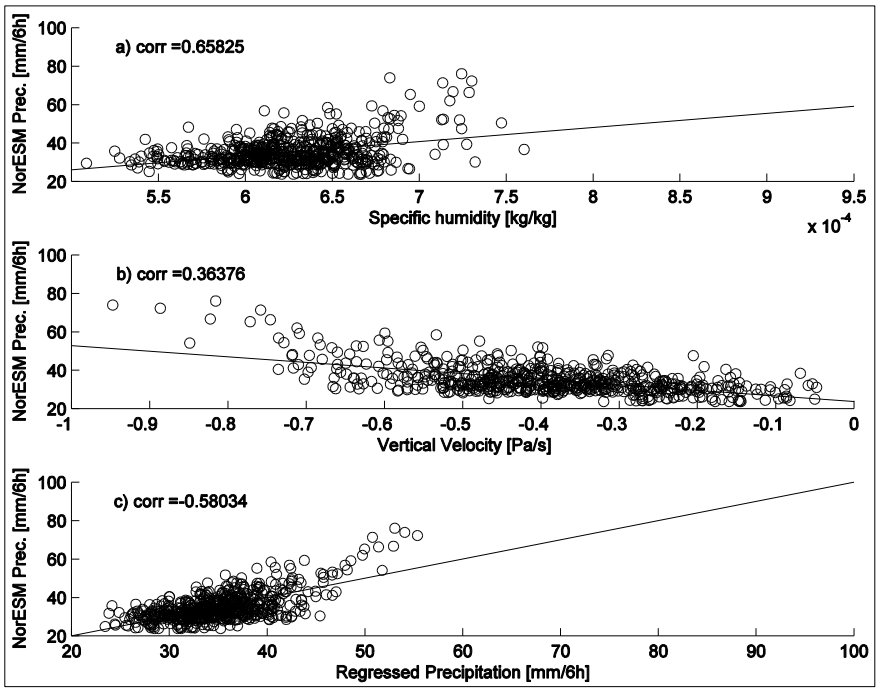

Figure 8.1: Scatterplot of 6-hourly NorESM Historical1 simulated extreme precipitation (y-axis) in Godavari contra a) integrated specific humidity, b) vertical velocity (omega), and c) extreme precipitation calculated from multiple linear regression. The black solid line indicates the least-square line of the scatter-data. Note that negative omega indicates ascent.

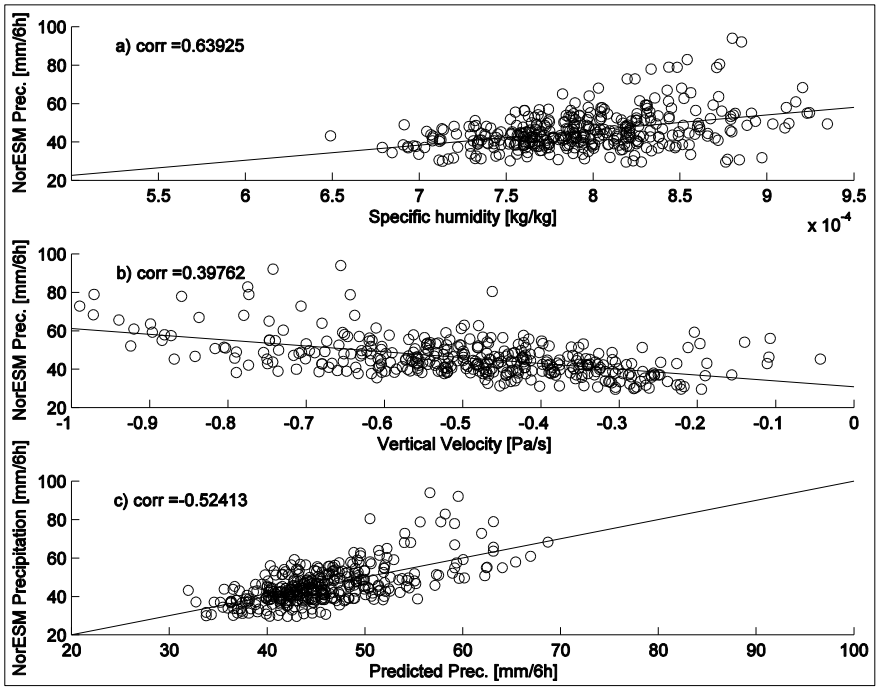

Figure 8.2: Scatterplot of 6-hourly NorESM RCP8.5 scenario extreme precipitation (y-axis) in Godavari contra a) integrated specific humidity, b) vertical velocity (omega), and c) extreme precipitation calculated from multiple linear regression. The black solid line indicates the least-square line of the scatter-data. Note that negative omega indicates ascent.

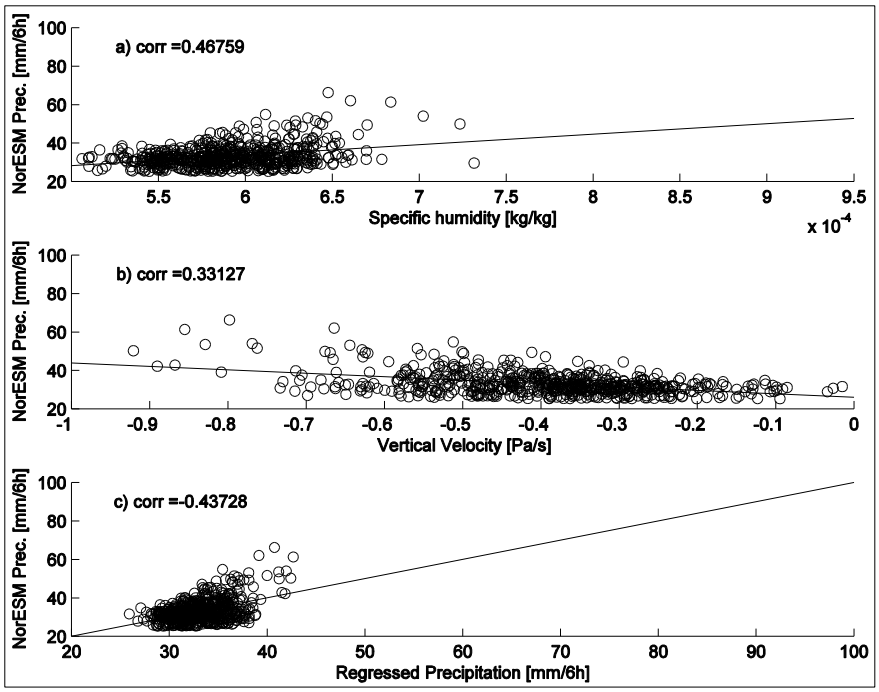

Figure 8.3: Scatterplot of 6-hourly NorESM Historical1 simulated extreme precipitation (y-axis) in Krishna contra a) integrated specific humidity, b) vertical velocity (omega), and c) extreme precipitation calculated from multiple linear regression. The black solid line indicates the least-square line of the scatter-data. Note that negative omega indicates ascent.

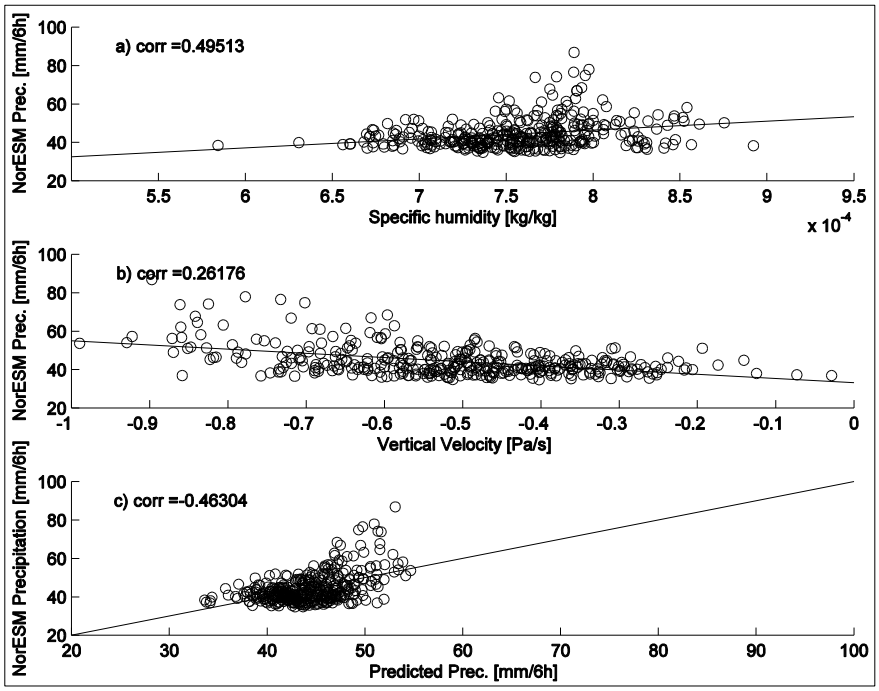

Figure 8.4: Scatterplot of 6-hourly NorESM RCP8.5 scenario extreme precipitation (y-axis) in Krishna contra a) integrated specific humidity, b) vertical velocity (omega), and c) extreme precipitation calculated from multiple linear regression. The black solid line indicates the least-square line of the scatter-data. Note that negative omega indicates ascent.

9. Summary and Conclusions

Throughout this thesis, the change in extreme precipitation, defined as the 99.5 percentile precipitation, between the period 1960-2000 and 2060-2100 is investigated. The Historical1 simulation from the NorESM is used for the historic values, while the RCP8.5 scenario from the same model covers the future period. Using values of temperature, horizontal winds and specific humidity, in addition to the calculated vertical velocity from the NorESM data, an attempt to explain why extreme precipitation occurs, in addition to the reason for the change in precipitation over the two periods, is done.

Over the last 40 years of the 19th century the yearly monsoonal extreme precipitation intensity and the yearly number of events with extreme precipitation is found to have a decrease, though no significant values are detected. However, comparing the mean yearly values of this period to the mean yearly values of the last 40 years in the 20th century, the trends show that both the mean intensity and the number of events will increase in the future. For the trends in the number of events per year there is a clear pattern where the trends become larger both with increasing periods (6-hour, day, 10-days), except for the monthly trends in which there are a drop in the trend compared to the other periods, and for increasing percentiles. For the yearly mean intensity, however, the values are found to be more even across different time periods, while an increase with percentiles are observed.

From the linear regression analysis, it is assumed that the vertical velocity and the specific humidity are the most important meteorological parameters in the formation of extreme precipitation during the monsoon. The vertical velocity has correlations of 0.44 and 0.58 with the extreme precipitation in the historic period over Godavari and Krishna, respectively, while the specific humidity has some lower correlations (0.40 and 0.30, respectively). The coefficients obtained from the equations of extreme precipitation variability also indicates that the vertical velocity is the most influencing parameter. Because the extreme precipitation occurs despite the stable temperature profiles during these events, the temperature is believed to have a minor impact on the formation compared to the vertical velocity and the specific humidity. In the future, all meteorological parameters will increase in magnitude, i.e. stronger vertical velocities, higher temperatures (with more stable profiles), and higher amounts of moisture, but the relationship between them related to their influence on the formation of extreme precipitation remains unchanged.

The simple model that only includes moist adiabatic ascent show that this simplification will result in too low precipitation amounts, especially within the 99.5 percentile. A possible explanation is the exclusion of diabatic cooling of the surrounding air, which increases the condensation rate in NorESM but not for the moist adiabatic estimate. However, the extreme precipitation trend in intensity show approximately the same values as in the NorESM, while the number of events is highly overestimated. The reason for a much higher rate of extreme events in the simple model compared to the NorESM may be that we assume the air to always be saturated in the simple model, and therefore it is able to produce precipitation much more often.

10. Future Work

As briefly mentioned in the introduction to Chapter 5, the thesis originally contained three other catchment areas; Brahmaputra, Ganges and Indus, but due to the poor performance of the NorESM model compared to APHRODITE and NCEP1, they were excluded. Brahmaputra was eliminated already in the validation of estimated precipitation due to a large overestimation in NorESM, while Ganges and Indus showed very weak correspondence with the NCEP1 vertical velocity. It will thus be interesting to know why Brahmaputra obtains too high precipitation amounts, and why the vertical velocity in Indus and Ganges show weak correlation with the observed vertical velocity despite the precipitation being satisfactory.

This thesis is based on a change in atmospheric variables resulting from the RCP8.5 scenario. Performing the same study on scenarios such as the RCP4.5 or the RCP6, it would be interesting to see how much the relative change in precipitation between future and historic periods would change, and if the vertical velocity and specific humidity still would be the dominating terms for the explanation of extreme precipitation variability. From the results obtained in Section 6.1.2, it would also be interesting to investigate why there is a drop in the relative change in precipitation intensity between the 95 and 99 percentile, as well as in the 99.9 percentile, as observed in Figure 6.6 and 6.7.

In terms of the global warming, the microphysics within clouds will also be affected. As more pollution occurs, the amount of aerosols in the atmosphere will increase, working as cloud condensation nuclei (CCNs, particles for water vapour to grow/condense on). Along with the estimated increase in water vapour in the atmosphere, an exploration of the type of processes occurring between water vapour and aerosols (e.g. condensation rate, collision between droplets) would be interesting regarding the effects on cloud amount and –depth, which will affect the radiation budget on the earth.

11. References

ADAMS, R. & ESSEX, C. 2009. *Calculus: A Complete Course*, Pearson and Prentice Hall.

ATTRI, S. D. & TYAGI, A. 2010. Climate Profile of India. *In:* CENTRE, E. M. A. R. (ed.). India: Indian Meteorological Department (IMD).

BENTSEN, M., BETHKE, I., DEBERNARD, J. B., IVERSEN, T., KIRKEV\AAG, A., SELAND, Ø., DRANGE, H., ROELANDT, C., SEIERSTAD, I. A., HOOSE, C. & KRISTJ\'ANSSON, J. E. 2013. The Norwegian Earth System Model, NorESM1-M – Part 1: Description and basic evaluation of the physical climate. *Geoscientific Model Development,* 6**,** 687-720.

BOOS, W. R. & KUANG, Z. 2010. Dominant control of the South Asian monsoon by orographic insulation versus plateau heating. *Nature,* 463**,** 218-222.

DEMOTT, C. A. & RANDALL, D. A. 2004. Observed variations of tropical convective available potential energy. *Journal of Geophysical Research: Atmospheres,* 109**,** D02102.

ESRL. 2015. *NCEP/NCAR Reanalysis 1: Pressure* [Online]. US Department of Commerce / NOAA. Available: http://www.esrl.noaa.gov/psd/data/gridded/data.ncep.reanalysis.pressure.html [Accessed 28.04 2015].

FUEGLISTALER, S., DESSLER, A. E., DUNKERTON, T. J., FOLKINS, I., FU, Q. & MOTE, P. W. 2009. Tropical tropopause layer. *Reviews of Geophysics,* 47**,** RG1004.

HARWOOD, R. S. 2006. Chapter 10: Vorticity and divergence. *Atmospheric Dynamics.* The University of Edinburgh.

HIRSCH, R. M., SLACK, J. R. & SMITH, R. A. 1982. Techniques of trend analysis for monthly water quality data. *Water resources research,* 18**,** 107-121.

HOUZE, R. A., WILTON, D. C. & SMULL, B. F. 2007. Monsoon convection in the Himalayan region as seen by the TRMM Precipitation Radar. *Quarterly Journal of the Royal Meteorological Society,* 133**,** 1389-1411.

JOHANSSON, E., DEVASTHALE, A., L'ECUYER, T., EKMAN, A. M. L. & TJERNSTRÖM, M. 2015. The vertical structure of cloud radiative heating over the Indian subcontinent during summer monsoon. *Atmos. Chem. Phys. Discuss.,* 15**,** 5423-5459.

KALNAY, E., KANAMITSU, M., KISTLER, R., COLLINS, W., DEAVEN, D., GANDIN, L., IREDELL, M., SAHA, S., WHITE, G., WOOLLEN, J., ZHU, Y., LEETMAA, A., REYNOLDS, R., CHELLIAH, M., EBISUZAKI, W., HIGGINS, W., JANOWIAK, J., MO, K. C., ROPELEWSKI, C., WANG, J., JENNE, R. & JOSEPH, D. 1996. The NCEP/NCAR 40-Year Reanalysis Project. *Bulletin of the American Meteorological Society,* 77**,** 437-471.

KITOH, A., ENDO, H., KRISHNA KUMAR, K., CAVALCANTI, I. F., GOSWAMI, P. & ZHOU, T. 2013. Monsoons in a changing world: a regional perspective in a global context. *Journal of Geophysical Research: Atmospheres,* 118**,** 3053-3065.

MARKOWSKI, P. & RICHARDSON, Y. 2011. *Mesoscale meteorology in midlatitudes,* John Wiley & Sons.

MILLERSVILLE UNIVERSITY. 2007. *Determining Meteorological Parameters from a Sounding* [Online]. Millersville University. Available: http://www.atmos.millersville.edu/~lead/SkewT_Parameters.html [Accessed 29.04 2015].

O'BRIEN, J. J. 1970. Alternative Solutions to the Classical Vertical Velocity Problem. *Journal of Applied Meteorology,* 9**,** 197-203.

O'GORMAN, P. & MULLER, C. 2010. How closely do changes in surface and column water vapor follow Clausius–Clapeyron scaling in climate change simulations? *Environmental Research Letters,* 5.

PALL, P., ALLEN, M. & STONE, D. 2007. Testing the Clausius–Clapeyron constraint on changes in extreme precipitation under CO2 warming. *Climate Dynamics,* 28**,** 351-363.

PRIVÉ, N. C. & PLUMB, R. A. 2007. Monsoon dynamics with interactive forcing. Part I: Axisymmetric studies. *Journal of the atmospheric sciences,* 64**,** 1417-1430.

SEN, P. K. 1968. Estimates of the regression coefficient based on Kendall's tau. *Journal of the American Statistical Association,* 63**,** 1379-1389.

SINCLAIR, M. R. 1994. A Diagnostic Model for Estimating Orographic Precipitation. *Journal of Applied Meteorology,* 33**,** 1163-1175.

SMITH, S. 1989. Water vapor flux at the sea surface. *Boundary-Layer Meteorology,* 47**,** 277-293.

SØRLAND, S. L. 2015. *Monsoon Low-Pressure Systems - The Precipitation Response to Atmospheric Warming.* PhD, University of Bergen.

STULL, R. B. 1988. *An Introduction to Boundary Layer Meteorology*, Springer Netherlands.

TURNER, A. G. & ANNAMALAI, H. 2012. Climate change and the South Asian summer monsoon. *Nature Climate Change,* 2**,** 587-595.

UEDA, H., IWAI, A., KUWAKO, K. & HORI, M. E. 2006. Impact of anthropogenic forcing on the Asian summer monsoon as simulated by eight GCMs. *Geophysical Research Letters,* 33.

UEDA, H. & YASUNARI, T. 1998. Role of Warming over the Tibetan Platean in Early Onset of the Summer Monsoon over the Bay of Bengal and the South China Sea. *JOURNAL-METEOROLOGICAL SOCIETY OF JAPAN SERIES 2,* 76**,** 1-12.

UPPALA, S. M., KÅLLBERG, P. W., SIMMONS, A. J., ANDRAE, U., BECHTOLD, V. D. C., FIORINO, M., GIBSON, J. K., HASELER, J., HERNANDEZ, A., KELLY, G. A., LI, X., ONOGI, K., SAARINEN, S., SOKKA, N., ALLAN, R. P., ANDERSSON, E., ARPE, K., BALMASEDA, M. A., BELJAARS, A. C. M., BERG, L. V. D., BIDLOT, J., BORMANN, N., CAIRES, S., CHEVALLIER, F., DETHOF, A., DRAGOSAVAC, M., FISHER, M., FUENTES, M., HAGEMANN, S., HÓLM, E., HOSKINS, B. J., ISAKSEN, L., JANSSEN, P. A. E. M., JENNE, R., MCNALLY, A. P., MAHFOUF, J. F., MORCRETTE, J. J., RAYNER, N. A., SAUNDERS, R. W., SIMON, P., STERL, A., TRENBERTH, K. E., UNTCH, A., VASILJEVIC, D., VITERBO, P. & WOOLLEN, J. 2005. The ERA-40 re-analysis. *Quarterly Journal of the Royal Meteorological Society,* 131**,** 2961-3012.

WALLACE, J. M. & HOBBS, P. V. 2006. *Atmospheric Science: An Introductory Survey,* University of Washington, Elsevier.

WAYNE, G. P. 2013. *Now available: a guide to the IPCC's new RCP emissions pathways* [Online]. The Guardian. Available: http://www.theguardian.com/environment/climate-consensus-97-per-cent/2013/aug/30/climate-change-rcp-handy-summary [Accessed 27.04 2015].

YASUTOMI, N., HAMADA, A. & YATAGAI, A. 2011. Development of a long-term daily gridded temperature dataset and its application to rain/snow discrimination of daily precipitation. *Global Environ. Res,* 15**,** 165-172.

YATAGAI, A., KAMIGUCHI, K., ARAKAWA, O., HAMADA, A., YASUTOMI, N. & KITOH, A. 2012. APHRODITE: Constructing a Long-Term Daily Gridded Precipitation Dataset for Asia Based on a Dense Network of Rain Gauges. *Bulletin of the American Meteorological Society,* 93**,** 1401-1415.

YUE, S. & PILON, P. 2004. A comparison of the power of the t test, Mann-Kendall and bootstrap tests for trend detection/Une comparaison de la puissance des tests t de Student, de Mann-Kendall et du bootstrap pour la détection de tendance. *Hydrological Sciences Journal,* 49**,** 21-37.

NCEP Reanalysis data provided by the NOAA/OAR/ESRL PSD, Boulder, Colorado, USA, from their Web site at http://www.esrl.noaa.gov/psd/